The Arecibo Legacy Fast ALFA Survey: II. Results of Precursor Observations

Riccardo Giovanelli[1], Martha P. Haynes[1], Brian R. Kent[1], Philip Perillat[2], Barbara Catinella[2], G. Lyle Hoffman[3], Emmanuel Momjian[2], Jessica L. Rosenberg[4], Amelie Saintonge[1], Kristine Spekkens[1], Sabrina Stierwalt[1], Noah Brosch[5], Karen L. Masters[1], Christopher M. Springob[1], Igor D. Karachentsev[6], Valentina E. Karachentseva[7], Rebecca A. Koopmann[8], Erik Muller[9], Wim van Driel[10], Liese van Zee[11]

ABSTRACT

In preparation for the full Arecibo Legacy Fast ALFA extragalactic HI survey, precursor observations were carried out in Aug–Sep 2004 with the 7-beam Arecibo L-band feed array (ALFA) receiver system and the WAPP spectral processors. While these observations were geared mainly at testing and debugging survey strategy, hardware and software, approximately 48 hours of telescope time yielded science–quality data. The efficiency of system usage (allowing for minor malfunctions and the impact of radio frequency interference) during that time was 75%. From those observations, an initial list of 730 tentative detections of varying degree of reliability was extracted. Ninety–eight high signal-to-noise candidates were deemed to be *bona fide* HI line detections. To test

[1]Center for Radiophysics and Space Research and National Astronomy and Ionosphere Center, Cornell University, Ithaca, NY 14853. *e–mail:* riccardo@astro.cornell.edu, haynes@astro.cornell.edu, bkent@astro.cornell.edu, amelie@astro.cornell.edu, spekkens@astro.cornell.edu, sabrina@astro.cornell.edu, masters@astro.cornell.edu, springob@astro.cornell.edu

[2]Arecibo Observatory, National Astronomy and Ionosphere Center, Arecibo, PR 00612. *e–mail:* phil@naic.edu, bcatinel@naic.edu, emomjian@naic.edu

[3]Hugel Science Center, Lafayette College, Easton, PA 18042. *e–mail:* hoffmang@lafayette.edu

[4]Harvard–Smithsonian Center for Astrophysics, 60 Garden St. MS 65, Cambridge MA 02138–1516. *e–mail:* jlrosenberg@cfa.harvard.edu

[5]The Wise Observatory & The School of Physics and Astronomy, Raymond & Beverly Sackler Faculty of Exact Sciences, Tel Aviv University, Israel. *e–mail:* noah@wise.tau.ac.il

[6]Special Astrophysical Observatory, Russian Academy of Sciences, Niszhnij Arkhyz 369167, Zelencukskaya, KChR, Russia. *e–mail*: ikar@sao.ru

[7]Dept. of Astronomy & Space Science, Kyiv University, Kyiv 252017, Ukraine. *e–mail:* vkarach@observ.univ.kiev.ua

[8]Dept. of Physics & Astronomy, Union College, Schenectady, NY 12308. *e–mail:* koopmanr@union.edu

[9]ATNF, CSIRO, PO Box 76, Epping, NSW 1710, Australia; *e–mail:* erik.muller@atnf.csiro.au

[10]Observatoire de Meudon, 5 Place Jules Janssen, 92195 Meudon, France. *e–mail:* wim.vandriel@obspm.fr

[11]Astronomy Dept., Indiana University, Bloomington, IN 47405. vanzee@astro.indiana.edu

our ability to discriminate cosmic signals from RFI and noise, 165 candidates ranging in reliability likelihood were re–observed with the single beam L–band wide system at Arecibo in Jan–Feb 2005. Of those, 41% were confirmed as real. We present the results of both the ALFA and single beam observations for the sample of 166 confirmed HI sources, as well as our assessment of their optical counterparts. Of the 166 sources, 62 coincide with previously known HI sources, while optical redshifts were available for an additional 18 galaxies; thus, 52% of the redshifts reported here were previously unknown. Of the 166 HI detections, 115 are identified with previously cataloged galaxies, of either known or unknown redshift, leaving 51 objects identified for the first time. Because of the higher sensitivity of the Arecibo system, fewer than 10% of the 166 HI sources would have been detected by a HIPASS–like survey of the same region. Three of the objects have HI masses less than 10^7 $M_\odot$. The full ALFALFA survey which commenced in February 2005 should detect more than 100 times as many objects of similarly low HI mass over the next 5 years.

Subject headings: galaxies: spiral; — galaxies: distances and redshifts — galaxies: halos — galaxies: luminosity function, mass function — galaxies: photometry — radio lines: galaxies

1. Introduction

The upgrade of the surface of the Arecibo antenna in the mid-1970's initiated a new era of extragalactic 21 cm HI line studies which exploited the big dish's collecting area and rapid progress in ancillary instrumentation (low noise amplifiers; broadband, flexible multi-bit spectrometers). Throughout the last 30 years, Arecibo observations have contributed to studies of large scale structure and the local peculiar velocity field, the dark matter content of galaxies and the impact of environment on galaxy evolution. The number of galaxies for which HI has been detected at Arecibo exceeds 10000, the vast majority of which have been studied via pointed observations of their optical counterparts using Arecibo's single beam feed systems. HI blind surveys conducted at Arecibo during the period of the upgrade by Zwaan *et al.* (1997; the Arecibo HI Strip Survey: AHISS) and by Rosenberg & Schneider (2000; the Arecibo Dual Beam Survey: ADBS) demonstrated the potential for discovery by the combination of Arecibo's high sensitivity and relatively small beam size, but were limited by the small areal coverage feasible with a single beam, surveying only 65 and 430 deg^2, respectively.

In addition to greatly increasing the sensitivity and reducing the frequency dependence of the Arecibo telescope, the Gregorian optical system installed in the 1990's delivered the possibility of extending Arecibo even further, through the installation of multi-feed arrays (Kildal *et al.* 1993). Similar systems at Parkes and Jodrell Bank have enabled the first full view of the extragalactic HI sky through the Parkes Multi-Beam HI Survey (HIPASS; Barnes *et al.* 2001) and the HI Jodrell

All-Sky Survey (HIJASS; Lang *et al.* 2003). The HIPASS catalog (HICAT; Zwaan *et al.* 2004, Meyer *et al.* 2004) includes 4315 detected HI sources over an area of 21341 deg^2. The advantages of Arecibo in terms of gain, angular and spectral resolution promise a significantly greater detected population, with much lower confusion probability and a deeper sampled volume, despite its more limited sky coverage ($-2^\circ < Decl. < +38^\circ$).

Most recently, the Arecibo telescope has been outfitted with a seven–beam 21 cm system dubbed the Arecibo L–Band Feed Array (ALFA). The combination of ALFA with the very large collecting area provided by the 305 m primary mirror now enables the undertaking of large area, high sensitivity surveys of the 21 cm sky to probe a variety of astronomical phenomena. To nurture the best use of ALFA for such large scale surveys, the National Astronomy and Ionosphere Center (NAIC) has fostered the formation of broad consortia, focused on separate science topics ranging from pulsar searches, to Galactic studies of continuum emission, the HI line and radio recombination lines, to extragalactic HI and OH line research. For extragalactic studies, the availability of ALFA renews the Arecibo legacy of high sensitivity, probing regimes untouched by other surveys and addressing fundamental cosmological questions (the number density, distribution and nature of low mass halos) and issues of galaxy formation and evolution (sizes of HI disks, history of tidal interactions and mergers, low z absorber cross section, origin of dwarf galaxies, nature of high velocity clouds).

The current authors constitute the initial team interested in exploring possibilities for conducting a blind HI survey of the nearby universe and thus came together to answer NAIC's call for initial survey precursor observations that would explore, develop and test optimal observing strategies, calibration schemes and data reduction pipelines. We have recently initiated a very wide area (7000 deg^2) blind HI survey: the Arecibo Legacy Fast ALFA (ALFALFA) survey. The ALFALFA program science goals and strategy are described in a companion paper (Giovanelli *et al.* 2005; Paper I). The precursor observations were carried out during the commissioning phase of ALFA and the data thus obtained do not lend themselves to a statistically accurate astronomical analysis. However, they provide an interesting new set of data and they allow for 'lower–limit' estimates of the potential of the ALFALFA survey, which we explore. We thus present those results and discuss how they aided us in adopting the final ALFALFA survey strategy.

In Section 2, we briefly discuss the observations made using the ALFA system as well as follow-up observations made with a single-pixel feed to test detection reliability. In Section 3, we present the parameters of HI detections. Their probable optical counterparts are identified in Section 4. Section 5 and Section 6 discuss the quality of inferred parameters and survey sensitivity. The final section summarizes the experience gleaned from the precursor observations discussed here in the context of the full ALFALFA survey as it is now being undertaken.

2. Observations

As part of the campaign to commission the ALFA instrument, NAIC issued a call for proposals in early 2004 for "precursor" programs that would engage the potential user community in the system commissioning. The observations reported here were carried out with the ALFA system in August and September 2004 under a "shared-risk" policy, allowing us to gain experience with the instrumentation, to test methodology and to develop software necessary for data management and processing. During this period, information about the ALFA system performance was accumulated and documented at the NAIC ALFA website[12]; a number of the memos posted there were contributed by members of this observing team. In this section, we briefly describe the configuration of the ALFA system and the observing mode adopted for the precursor observations. More details on the system can be found in Paper I. It should be noted that the system and our approach have evolved since the precursor observations were undertaken, partly in response to the experience gained through them.

2.1. ALFA Observations

Given the "shared risk" character of these early ALFA observations, a large fraction of the telescope time was used to test and optimize data-taking procedures and to debug and calibrate the new system. Data in "survey mode" were obtained for a total of 47.8 hours, albeit a fraction of those were affected by several problems. Among the problems encountered during this "shakedown" period were the loss of one of the polarization channels on the central pixel (beam 0); strong, permanent and internally generated radio frequency interference (RFI) on the other polarization channel of beam 0; transient, internally generated RFI with drifting frequency over all beam/polarization channels (the 'wandering birdie'); strong external RFI, mixing selectively at different frequencies in each backend board; the effects of dynamically evolving data taking software. Most of those problems were resolved or largely attenuated towards the end of or after our precursor run. The efficiency of telescope usage over the 47.8 hours of our observations in survey mode during this observing session was $\simeq 75\%$. One important consequence of the problems encountered was the unevenness of the sky coverage on small scales and an impact on the statistical homogeneity of the data sets.

The gain of the seven beams of ALFA ranges between 8.5 and 11 K Jy^{-1}, and the system temperatures range between 26 and 30 K on cold sky (including atmosphere and Cosmic Microwave Background emission).

All the survey mode observations were made with the telescope stationed at azimuth=180°, thus enabling observations of the sky north of the Arecibo zenith. The feed array (see Paper

[12] *http://alfa.naic.edu/memos*

I for a description) was rotated to an angle of 19° from its nominal rest alignment, yielding a configuration in which the sky footprints of its seven individual beams sweep tracks on the sky equally spaced in Declination, as the Earth rotates. The spacing of the beams in this configuration is $\sim$2.1′ (126″), slightly worse than Nyquist, as the beams have elliptical half power full size of 3.3′×3.8′. Drift scans of 900 seconds duration were taken sequentially, with about 3–4 seconds of dead time between one scan and the next. The duration of each drift was dictated by the need to obtain individual data files of manageable size and to minimize data loss in case of equipment malfunction. A successive set of drifts was obtained with minimal interruption. It should be noted that under the constraints of telescope control during the 2004 precursor period, the beams followed tracks of constant declination at the current epoch, although initial positioning was commanded to J2000 Declination. ALFALFA observations in 2005 allow for periodic adjustments to maintain a constant J2000 Declination.

The backend spectrometer system consisted of a set of four WAPPs (Wideband Arecibo Pulsar Processor), which allowed instantaneous autocorrelation and sampling of 16 time series, each yielding a 100 MHz wide spectrum of 4096 channels. Fourteen of those were used to process and record the two independent polarization channels of each of the seven beams of ALFA. The remaining two recorded redundant data and the resulting data buffers were subsequently used by us to record the median of all the 7 beams, as a tool for RFI monitoring. The spectral resolution of 25 kHz corresponds to $R = \lambda/\Delta\lambda \simeq 57,000$, or 5.3 km s^{-1}, at the 1420 MHz rest frequency of the HI line. All spectra were centered at a frequency of 1385 MHz, in the Observatory reference frame, i.e. no Doppler tracking was implemented to allow for the varying component of the Earth's motion with respect to a cosmic reference frame. A heliocentric correction was computed and applied to the data during the off–line processing stages, using an IDL routine developed by one of us (PP) and C. Heiles. The effective spectral coverage of the data was restricted to the interval between 1342 to 1428 MHz, due to the drop in sensitivity of the backend near the band edges. Further losses of spectral coverage resulted from RFI, as described in the next section. The range of radial velocities corresponding to that frequency interval, for the HI line, is cz = [17500 to −1600] km s^{-1}. That interval thus includes the HI emission of the Milky Way and of perigalactic High Velocity Clouds, as well as the rest frequency of several radio recombination lines.

Data were recorded every second; thus a 900 second drift consists of 900 records, each of sixteen, 4096 spectral channel spectra (two polarizations for each of the 7 ALFA beams plus one spare pair). A drift is made up of $900 \times 8 \times 2 \times 4096$ spectral samples, each 4 bytes long, plus header information, adding up to about 0.25 GByte. This configuration differs from the ALFALFA survey currently under way, for which drifts are 600 seconds long. The change was made in order to better accommodate the gain calibration scheme, which evolved from that adopted during the precursor observations.

The sky coverage of the precursor run observations is shown in Figure 1. Part of the region, extending near 100° in R.A. but confined to a swath only 0.5° in Declination. This region was covered in "single–pass" mode, i.e. only one set of drift scans swept any part of the sky, with the

Declination tracks of each beam separated from one another by $\sim 2.1'$. A $30^\circ \times 1.8^\circ$ region was (almost) covered in "two–pass" mode, whereby a second set of drift scans was obtained, sweeping over the same region of sky during a separate observing session. During the second pass, the center beam pointing shifted $7.3'$ in Declination. In this case, as evident in Figure 1, the Declination sampling is twice as dense ($1.05'$), and the scalloping that arises from the fact that the central beam has higher gain is smoothed somewhat. The second mode is representative of the strategy adopted for the full ALFALFA survey (see Paper I).

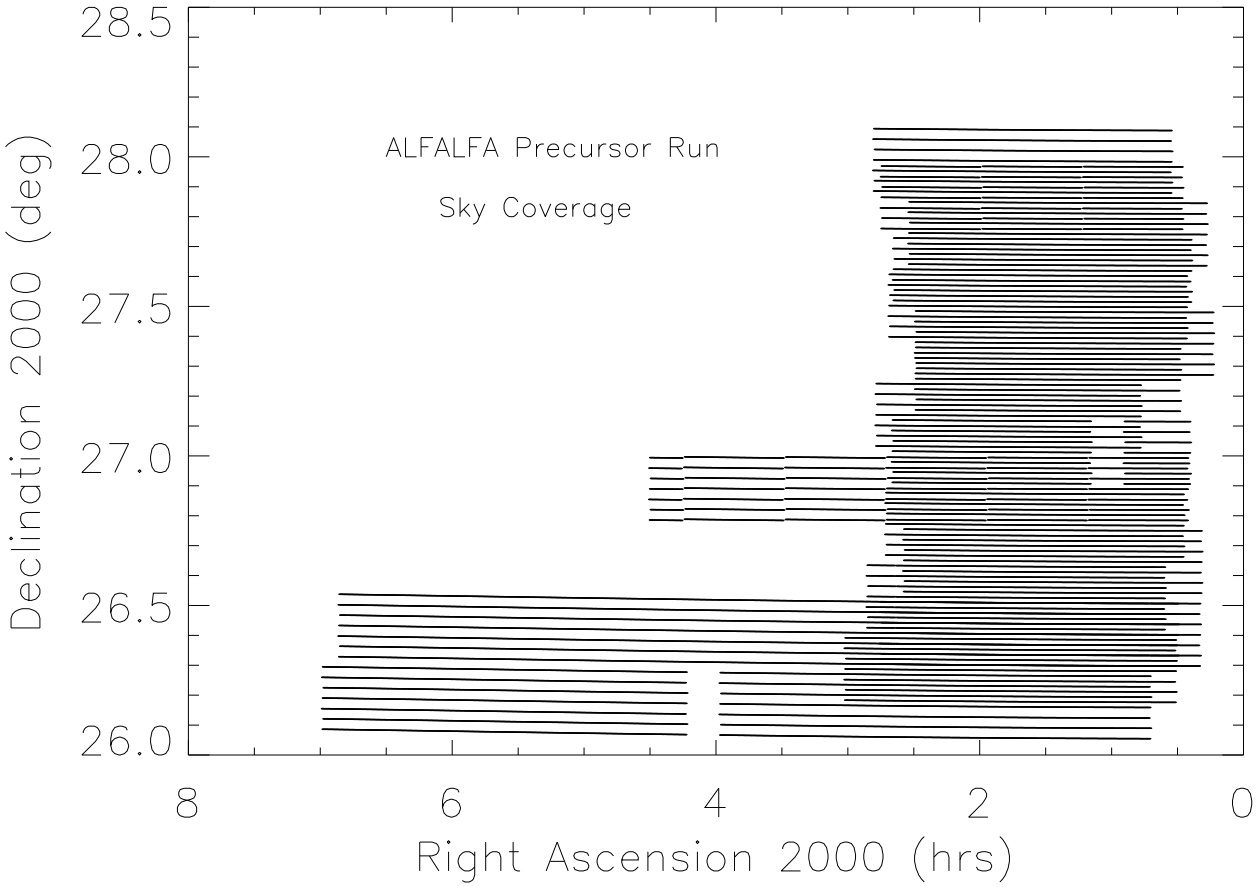

Fig. 1.— Region sampled by the ALFALFA precursor run discussed in this paper. Individual beam tracks for each drift are outlined by sequences of dots at constant Declination. Tracks in "single–pass" regions are spaced $2.1'$ in Declination, while those in 'two–pass' regions are spaced $1.05'$ in Declination. Many gaps in local coverage are present on small scales. For the full ALFALFA survey, sampling will be more homogeneous.

A noise calibration diode which increased the system power by about a third was fired for one second every 275 seconds during data taking. This turned out to be an inconvenient choice, for the duration of the calibration was unstable, yielding spurious calibration results. In latter parts of the run, the calibration diode was fired for 2 seconds, assuring that the noise diode was "on" for at least

one full record. In that instance, 4 seconds (records) of data were lost and interpolated across during data processing. The stability of the noise calibration was checked by monitoring the polarization ratios of the Galactic HI line, which falls within the observed bandwidth, and by monitoring the ratios of that line's intensity among the various beams, which stochastically should remain constant in a stable system (Giovanelli *et al.* ALFALFA memo[13]). Drifts in the calibration values of up to 4% were observed, over the period of about one month of the precursor run observations. The final flux density scale on which the results reported here are based is estimated to be accurate to within 4%. Analysis of the continuum data for sources within the region surveyed is currently under way and is expected, when completed, to allow us to tighten the calibration of the flux density scale of the ALFALFA dataset to within 1–2%.

2.2. The Radio Frequency Interference Environment

Several known sources of RFI polluted the observed spectral band, as well as several unexpected ones. The most prominent among those is the FAA radar at 1350 MHz, which rendered useless an interval of variable width, averaging approximately 150 spectral channels (nearly 4 MHz). Our observations are thus "blind" to HI sources redshifted to cz between about 15,200 and 16,000 km s^{-1}. RFI features related to the FAA radar also appeared at 1380 MHz about 90% of the time, affecting some 30 spectral channels, and with lower impact and intensity at other frequencies as well. Downlink transmission by the Global Positioning System (GPS) constellation of satellites affected data between 1378 and 1384 MHz for irregular intervals of approximately 100 seconds, every few hours. Other sources of RFI external to the Observatory occasionally affected a large and variable number of frequencies throughout the run. The estimated reduction in the usage efficiency of the 86 MHz surveyed band (after exclusion of the band skirts) due to external sources of RFI is about 10%.

Several internal sources of RFI were identified during the precursor run. Most insidious was a feature of drifting frequency and relatively low intensity, which affected the spectral region between 1385 and 1420 MHz. This "wandering birdie" occurred erratically throughout all our precursor run and was locally generated. Fortunately, its source was finally identified and corrected in early 2005. At least 5% of our precursor data were irrecoverably marred by this feature. Other RFI features were found to be localized within a single WAPP. One polarization channel of the central beam of ALFA was malfunctioning and thus unavailable during most of the precursor observations, while the other polarization channel of the same beam exhibited a strong RFI feature some 10 MHz wide centered near 1384 MHz.

The overall reduction of efficiency of usage of the 86 MHz surveyed spectral band, due to the combined effect of external and internal sources of RFI and partial (i.e. affecting only minor parts

[13] *http://www.astro.cornell.edu/∼haynes/pre204/docs/memo040920.pdf*

of the equipment but maintaining most capabilities intact) hardware malfunction, is estimated to have been 25%, over the 47.8 hours of telescope time in survey data taking mode. Because several of these RFI sources have been subsequently eliminated, efficiency in the ALFALFA dataset will be considerably higher. This expectation is being confirmed by the early runs of the survey.

The inspection of data in a "global" framework, i.e. as maps rather than assemblies of individual spectra, is an absolute necessity in gauging the likelihood that any signal be of cosmic origin rather than noise or RFI. We developed an algorithm that maintains a dynamic memory of RFI features, flagging spectral regions of locally enhanced RFI activity and "unflagging" them as RFI becomes statistically quiescent. While the technique does not guarantee total reliability in the assessment of the nature of any given signal, it helps exclude the vast majority of spurious ones quite effectively. Further development of this approach will be a necessity in the analysis of the ALFALFA survey data in order to maximize its efficiency and reliability.

2.3. Confirmation Observations

As the signal-to-noise of candidate detections decreases, their contamination by spurious noise "signals" in a survey such as ALFALFA quickly rises. Detection algorithms must thus be optimized to discriminate real from spurious signals as well as possible. In early February 2005, 14 hours of telescope time were scheduled with the Arecibo single pixel L–band wide (LBW) feed system to test the results of detection reliability simulations (see Paper I) through confirmation of ALFA detection candidates. Observations were scheduled in the late afternoon and early evening. This time of day is notoriously bad for broad–band spectral line observing due to the rapidly varying pattern of standing waves originating from solar radiation. Observing time was available in small slots between previously scheduled programs. Rather than waiting for the LST period associated with the precursor ALFA observations to shift to a more advantageous part of the diurnal cycle, i.e. the second half of the year, we used the available segments of telescope time, adopting measures to minimize the impact of standing wave variations. The usage of the time was thus not optimal, but we could observe 165 detection candidates, spanning a range of reliability likelihood, in a timely manner.

The gain of LBW is 11 K Jy^{-1} near 1385 MHz and its system temperature on cold sky is 27 K, with small variations about these values resulting from the telescope configuration. All detections were confirmed by LBW observations at zenith angles of less than 15°, for which gain and temperature variations are within a few percent.

The LBW observations were made with the same spectrometer backend used for the ALFA observations, covering a spectral band of 100 MHz, centered near 1385 MHz. The early part of the LBW observations were made with 8192 spectral channels, while the latter part of the run adopted an observing mode change to 4096 spectral channels (to circumvent a software bug), which respectively yielded channel separations of about 2.5 and 5 km s^{-1}. All data were smoothed to the

same spectral resolution of 10 km s^{-1}, before measurement of detected features.

Integration times for ON source observations varied between 1 and 3 minutes. They were both preceded and followed by OFF source observations of comparable duration, so that only one third of the integration time was on source. The quality of the spectral baselines remained poor, albeit far superior to those obtained with the traditional, one–sided ON–OFF pattern commonly used for extragalactic, spectral line pointed observations. Evidence of the impact of standing waves on this data is conspicuous in our spectra. Nonetheless, confirmation of 68 candidate ALFA detections was possible.

3. Results

In addition to providing an opportunity to shakedown the hardware and software associated with the new multi-beam system, the precursor observations also produced a spectral dataset to verify ALFA's true efficacy for extragalactic science. To process the ALFA spectral line dataset, we have adopted the IDL processing environment and have made use of the suite of general purpose analysis tools available at the Arecibo Observatory as well as new ones developed by us specifically for ALFALFA. The raw spectral data were converted from the FITS format delivered by the data acquisition software to the form of IDL structures adopting the format defined in previous years at NAIC by one of us (PP). While some details of the data processing refer only to the present precursor dataset, given that system changes have taken place since the commissioning phase, the basic approach to data analysis follows that discussed for the full ALFALFA survey as presented in Paper I.

In this section, we describe separately the HI detections extracted from the ALFA drift observations and from the targeted LBW follow-up. Table 1 summarizes the results' statistics, which are described below. Spectra, images of optical counterparts and tabulated information on these data can be access through the web directly [14], or through the ALFALFA website[15].

3.1. ALFA Detections

Individual drift scans were processed through several distinct stages. The first consisted of bandpass subtraction, calibration and baselining; this step also produced continuum time series for each beam. The spectral line data output of this stage is in the form of baselined arrays of spectra, ready for individual inspection as position–velocity (time–frequency) images. The construction of 3D maps, resulting from the combination of drift tracks at different Declinations, was not possible

[14] *http://egg.astro.cornell.edu/precursor*

[15] *http://egg.astro.cornell.edu/alfalfa*

with effectiveness with the precursor run data, because of the numerous gaps in the data streams and deficiencies in the data quality. The data were thus visually inspected by one of us (RG) — one drift track at a time — after spatial smoothing to an effective integration time of $t_s = 14$ sec, which yielded position-velocity maps with a median rms noise of $3.5 \times (res/10)^{-1/2}$ mJy, as described in Paper I, where res is the spectral smoothing window in km s^{-1}. The data of single drift maps were smoothed at various resolution levels, before inspection. After signal identification, features identified in more than one beam track were accumulated using a Gaussian weighting function of $2'$ half power kernel, smoothed to a resolution of 16 km s^{-1}and measured to obtain velocities, widths and flux integrals, to a resolution varying between 11 and 16 km s^{-1}. The cross–referencing of the candidate detections among contiguous beam tracks was made after signal identification, obtaining corroborating evidence for each candidate source. While this approach improved the final signal–to–noise ratio, it did *not* play a role in the initial identification of detection candidates. An automated matched filter signal extraction algorithm which operates in the Fourier domain is currently being applied to the data; visual and automated source detections are being compared to calibrate the threshold of the algorithm. Its results will be presented in a later report (Saintonge *et al.* in preparation).

An initial list of 730 candidate detections was obtained through the process described above; these ranged in quality from highly probable detections to very low signal-to-noise candidates, the majority of which are not likely to be real. The identification of such a large list at this stage was made specifically for the purpose of testing signal verification techniques. Of the 730 initial candidates, 98 were deemed to be reliable detections to a high level of confidence, either because their existence was previously known or because the corroborating evidence of detection in several beams was strong and of high signal–to–noise. They were not reobserved. Of the remaining less certain detections, 165 candidates were reobserved in the confirmation run in early February 2005, with the single pixel LBW feed at Arecibo, as reported in the next section. Priority was given to those deemed most likely to be real, but a range of candidates were included in the followup observations. Sixty–eight of the reobserved candidate detections were confirmed, for a confirmation rate of 41%. The remaining 467 candidate sources have not been reobserved and will not be discussed further in this preliminary report. These statistics are summarized in Table 1.

Whenever possible, a region of typically 100 square arcminutes around each of the candidate sources within the precursor dataset was inspected and a map of the total HI emission in that region was produced, yielding a centroid position and a total HI line flux integral. Because of the uneven sky coverage of the precursor run, many of the regions surrounding candidate detections were only sparsely sampled, as noted in the comments to the tabulated data below and in the large variations in the resulting sensitivities. As described before, for each candidate detection a composite spectrum was produced and a centroid extracted, after combining data from all spectra within several arcminutes radius from the centroid position, with each spectrum weighed according to a Gaussian kernel which was equivalent to smoothing the data from the $3.3' \times 3.8'$ telescope beam size to a circular beam of $4'$ full width at half power. The rms noise as measured in this

coadded spectrum is tabulated as described below, after spectral smoothing of between 11 and 16 km s^{-1} resolution. The HI line flux integral, center velocity and spectral width were measured on each composite spectrum; they are listed in Table 2. Whenever the flux integral obtained from the map yielded significant evidence for emission extended in comparison with the beam size, that value is also reported in Table 2. In the vast majority, the confirmed detections are weak. The possible impact of sidelobe contamination on each source was checked by inspection of the vicinity of each candidate detection.

For the few large, highly extended sources, such as HI 014729.9+271958 (IC 1727) and HI 014753.9+272555 (NGC 672), for which a detailed study of the HI extent and characteristics is warranted, we defer to a later report. Spectral line profiles of each detected source, after coaddition and smoothing as described above, can be accessed via the web through the aforementioned sites.

Table 2 contains the parameters derived from the ALFA HI data, namely:

- Col. 1: source name, composed of the qualifier 'HI' and the R.A. and Dec. (epoch J2000.0) of the HI centroid.

- Col. 2: estimates of the errors in the measurement of the centroid position, respectively in seconds of time for the R.A. (ϵ_α) and in seconds of arc for the Declination (ϵ_δ).

- Col. 3: center heliocentric velocity cz of the feature and estimate of the measurement error on cz, ϵ_{cz}, in km s^{-1}; when two non zero numbers are listed for ϵ_{cz}, the second is an estimate of the systematic component of the error, while the first is a statistical error which depends on the shape of the signal and the signal–to–noise. The systematic error results from the observer's subjective choice of the signal boundaries: when those are clear, the systematic error is nil; when strong uncertainty exists in making that choice, a visual guess is made by the observer of the potential amplitude of the uncertainty. The total error on cz is the sum in quadrature of the two components of the error.

- Col. 4: velocity width of the spectral feature, in km s^{-1}, measured at 50% level of intensity of two peaks on each side of the signal and its associated estimate of error, ϵ_w. Note that the measurement error on the width is effectively a fractional error, so that $W(\epsilon_w) = 100(50)$ should be read as 100^{+50}_{-33}. Widths are corrected for instrumental smoothing and relativistic broadening, i.e. the tabulated values are $(W^2_{measured} - res^2)^{-1/2}/(1+z)$, where res is the spectral resolution in km s^{-1}. No disk inclination nor turbulent motion correction is applied to the widths.

- Col. 5: rms of the composite HI spectrum, in mJy, measured 'locally', i.e. over a baseline region within 10 MHz of the detected feature rather than over the full spectrum.

- Col. 6: Flux integral of the spectral feature measured on the composite spectrum F_c, in Jy km s^{-1}, and its associated statistical error, ϵ_f, compounded with the overall uncertainty on

the flux calibration. This value is an underestimate of the true flux if the source is extended in comparison with the beam size.

- Col. 7: In cases for which the ALFA data indicate significant angular extent of the HI source, an estimate of the total flux of the source derived from a map, F_m is given. Note that for the majority of sources the signal–to–noise ratio is not sufficient to obtain a reliable map.

- Col. 8: A letter "L" indicates that the ALFA detection is corroborated by observations with the LBW single–pixel feed. The results of those observations are given in Table 3. An asterisk in this column indicates that comments are available for the given source.

3.2. LBW Detections

As stated in Section 2.3, follow-up observations made with the single-pixel LBW system were conducted in several small blocks of telescope time under far from optimal observing conditions, to test the reliability of candidate detection of low signal-to-noise. The LBW observations were generally centered on the position of what was initially identified as the optical counterpart of the HI source. In some cases, additional observations on alternative interpretations of that association were made, to ascertain its reality. The results are presented in Table 3, which lists:

- Col. 1: source name, as given in Table 2, with coordinates referred to the centroid of the ALFA observations.

- Cols. 2, 3: Right Ascension and Declination of the LBW observation, epoch J2000.0.

- Col. 4: center heliocentric velocity cz of the feature, and estimate of the error on cz, ϵ_{cz} in km s^{-1}, defined as described for the analogous quantities in Table 2.

- Col. 5: velocity width of the spectral feature and related uncertainty, in km s^{-1}, as described in Table 2.

- Col. 6: rms of the HI spectrum, in mJy, measured 'locally', i.e. over a baseline region within 10 MHz of the detected feature rather than over the full spectrum.

- Col. 7: flux integral and related uncertainty, in Jy km s^{-1}.

- Col. 8: an asterisk indicates that comments are available for the source.

Entries in Table 3 are cross–referenced in Table 2 by the presence of an "L" in Col. 8 of that table. Spectra can be accessed through the aforementioned websites.

4. Identification of Optical Counterparts

Fields of $10' \times 10'$ around each HI detection were inspected for optical counterparts, using DSS2 via *Skyview*[16], NED[17] and our privately maintained data base of extragalactic sources (the "AGC", for "Arecibo General Catalog"). Optical counterparts are identified for all but 4 of the 166 confirmed HI sources. In a few cases, the identification of an optical counterpart is ambiguous, as noted below. In at least one of those cases (HI 062218.4+262631), the simplest explanation for the lack of an optical counterpart is that the source region is affected by high optical extinction, in the vicinity of the galactic plane. Table 4 lists the positions of the proposed optical counterparts, as follows:

- Col. 1: source name, as in Table 2.
- Col. 2: catalog number in the AGC; AGC numbers smaller than 13000 coincide with those of the Uppsala General Catalog (Nilson 1973).
- Col. 3,4: Right Ascension and Declination (epoch J2000.0) of the proposed optical counterpart of the HI source. These coordinates are either obtained from previous tabulations or directly measured using the *Skyview* facility. Positional accuracies are of order $1''$.
- Col. 5: Source distance in Mpc, D_{cmb}, obtained from the radial velocity corrected to the Cosmic Microwave Background rest frame, and assuming pure Hubble flow with $H_\circ = 70$ km s^{-1} Mpc^{-1}.
- Col. 6: Source distance in Mpc, D_{pec}, obtained from the measured redshift and from the peculiar velocity field model of Tonry *et al.* (2000), for $H_\circ = 70$ km s^{-1} Mpc^{-1}. In addition to the error on the measurement of cz and the systematics in the flow model (see Masters 2005), a "thermal" velocity component of 187 km s^{-1} as assumed by Tonry et al. (2000) introduces an additional uncertainty of 2.7 Mpc on each distance estimate.
- Col. 7: logarithm in base 10 of the HI mass M_{HI}, expressed in solar units via $M_{HI} = 2.356 \times 10^5 D^2 \times F$, where D is the distance in Mpc given in Col. 6 and F is the flux integral obtained from Col. 7 (or Col. 6 if Col. 7 is blank) of Table 2.
- Col. 8: an asterisk indicates that comments are available for the source.

Notes associated with the objects listed in Tables 2, 3 and 4 follow:

---

[16] *Skyview* was developed and maintained under NASA ADP Grant NAS5–32068 under the auspices of the High Energy Astrophysics Science Archive Research Center at the Goddard Space Flight Center Laboratory of NASA.

[17] The NASA/IPAC Extragalactic Database (NED) is operated by the Jet Propulsion Laboratory, California Institute of Technology, under contract with the National Aeronautics and Space Administration.

HI 001709.7+271616: sparse sampling; HI Dec. poorly constrained.

HI 002115.8+262318: Marginal LBW confirmation due to standing waves of solar radiation.

HI 002312.5+272644: previous HI det at cz=3905.

HI 002818.8+272136: previous HI det at cz=9608.

HI 002905.1+272913: beware: feature v. near transient RFI.

HI 003855.1+265753: previous HI det at cz=5192.

HI 004034.8+270239: 2MASS object at 004042.3+270243, but opt id more likely with larger, uncatalogued lsb galaxy nearby.

HI 004256.8+271522: previous HI det at cz=5289.

HI 004357.1+260731: previous HI det at cz=4898. Checked for HI emission on gal. at 004349.8+261113: negative. Optical id as given in table confirmed.

HI 004404.2+261243: marginal, but matches previous HI det at cz=10082.

HI 004411.5+265042: previous HI det at cz=5187; extended HI.

HI 004645.5+275553: ALFA detection superimposed on RFI; while easily identified on position-velocity map of drift, flux, width and centroid very unreliable. LBW data cleaner, corroborated by previously measured cz of 6893 for CGCG 500-088.

HI 004650.7+262846: previous HI det at cz=4954.

HI 004716.1+274854: previous HI det at cz=4742.

HI 004803.3+273717: marginal detection, corroborated by previous HI det at cz=4949.

HI 004816.9+262806: previous HI det at cz=5269.

HI 004834.5+274100: previous HI det at cz=5214.

HI 005009.5+271328: previous HI det at cz=4922.

HI 005305.3+272909: 2MASS object at 005310.1+272837, but opt id more likely with larger, uncatalogued lsb galaxy nearby.

HI 010158.0+263010: previous HI det at cz=10069.

HI 010225.7+263713: previous HI det at cz=4992.

HI 010318.1+264747: opt id is double system; HI profile shows evidence of blend. 2MASS object at 010321.4+264737, but opt id more likely with larger, uncatalogued lsb system nearby.

HI 011302.6+273832: Checked for HI emission on gal. at 011309.8+273925: negative. Optical id as given in table confirmed.

HI 011443.5+270813: previous HI det at cz=3618.

HI 011743.9+270006: 2MASS object at 011737.0+265902, but opt id more likely with larger, uncatalogued lsb galaxy nearby.

HI 012242.5+265157: close pair of gals (Mark 355/6, CGCG 481-004) at (a) 012240.8+265206 and (b) 012243.1+265200, previously measured cz: 9187, 9068; optical id given as center of pair; HI centroid marginally favors id with (b).

HI 012403.9+270300: previous HI det at cz=4917.

HI 012405.2+280433: sparse sampling; HI Dec. poorly constrained.

HI 012607.5+275810: merging pair; previous HI det at cz=4021.

HI 012944.1+272249: sev. opt candidates in field, most notably: (a) 012943.6+272340 and (b) 012947.0+272220, merging pair; (b) is IRAS F01270+2706, with opt cz of 12566, matching HI cz. Nonetheless, optical id remains ambiguous.

HI 013716.0+262605: previous HI det at cz=3872.

HI 014105.8+272007: checked for emission with LBW 1 beam off N,S,E,W; source not significantly extended.

HI 014147.3+273159: marginal detection, corroborated by previous HI det at cz=10828.

HI 014214.9+262202: previous HI det at cz=359.

HI 014428.3+275522: previous HI det at cz=4037.

HI 014441.4+271707: previous HI det at cz=420.

HI 014455.3+272942: marginal det by ALFA.

HI 014640.9+264754: previous HI det at cz=361.

HI 014653.7+280448: marginal ALFA detection, corroborated by previously measured opt cz=3590.

HI 014724.3+275312: NGC 670; previous HI det at cz=3703.

HI 014729.9+271958: IC 1727, v. extended, blends with NGC 672; HI flux integral much larger than tabulated central beam flux. Accurate flux integral will require detailed study.

HI 014753.9+272555: NGC 672, v. extended, blends with IC 1727; HI flux integral much larger than tabulated central beam flux. Accurate flux integral will require detailed study. Primary distance of 7.9 Mpc available.

HI 014837.9+273259: close pair (CGCG 482-017), with (a) 014835.2+273253 and (b) 014835.3+273326, opt. cz=10979; HI centroid very marginally favors id with (a).

HI 014915.3+274248: previous HI det at cz=10753.

HI 015011.6+271145: previous HI det at cz=3502.

HI 015013.0+273842: previous HI det at cz=3537.

HI 015439.8+271111: RFI excised from edge of feature in ALFA spectrum.

HI 015519.2+275645: KK16; previous HI det at cz=206. Primary distance of 4.7 Mpc available.

HI 015917.6+270027: previously measured cz=5309.

HI 015937.0+272555: previous HI det at cz=5267. Extended, but HI map corrupted, unable to obtain total flux.

HI 015952.5+262407: opt counterpart is chain of merging units.

HI 020133.9+262914: merging pair; previous HI det at cz=5146.

HI 020144.4+263227: previous HI det at cz=5001.

HI 020248.2+263434: previous HI det at cz=14593.

HI 020304.8+271222: sev. starlike features in field, but no unambiguous optical counterpart identified. Different interpretations of spectral extent of signal adopted in ALFA and LBW spectra. Marginal det.

HI 020329.8+273909: highest cz of detections list.

HI 020343.0+261608: previous HI det at cz=5014. Only 4' away from HI 020353.5+261719. Peak fluxes suggest that sidelobes do not play role in detection.

HI 020353.5+261719: Only 4' separation from HI 020343.0+261608. Peak fluxes suggest that sidelobes do not play role in detection.

HI 020430.7+275454: previous HI det at cz=4699.

HI 020626.5+270152: previous HI det at cz=4964.

HI 020902.1+273202: previous HI det at cz=9856.

HI 020913.9+264536: marginal detection, marginal confirmation with LBW.

HI 020954.1+273147: triplet of small units; opt id tentatively assigned to largest unit.

HI 021404.3+275302: UGC 1718 = NGC 855 at opt. cz=594, classified as Elliptical. Small spiral at 021405.8+275034: LBW observation centered on it yields much lower flux integral. Most likely optical id is UGC 1718; however, classified as elliptical, the galaxy is more likely a star-forming dwarf with a central bar and some young star clusters.

HI 022102.1+274615: two 2MASS galaxies within 2.5', but larger, uncatalogued object is better match as opt. counterpart.

HI 022103.9+270204: marginal ALFA detection, marginal LBW confirmation.

HI 022224.8+262552: previously measured opt cz=11179.

HI 022335.8+271851: marginal detection corroborated by previous HI det at cz=10645.

HI 022340.2+270927: previous HI det at cz=10647.

HI 022348.9+272848: previous HI det at cz=10706.

HI 022355.8+270618: previous HI det at cz=5470.

HI 022405.6+263900: sev. small LSB features in field, most notably: (a) 022402.0+263958 and (b) 022408.9+263952; optical id ambiguous.

HI 022459.4+260314: marginal detection corroborated by previous HI det at cz=10080.

HI 022533.4+264458: previous HI det at cz=10348.

HI 022538.8+271709: previous HI det at cz=8984.

HI 022558.5+271607: 2MASS galaxy with measured opt. cz=10493; in group with NGC 916 at 022547.6+271432, cz=9614. Marginal HI parameters.

HI 022609.4+273549: previous HI det at cz=9980.

HI 022617.1+260750: peculiar (double) gal (CGCG 483-047) at opt. cz=10128. Marginal HI det.

HI 022620.2+271315: Very marginal ALFA detection, corroborated by previous HI det at cz=10357.

HI 022629.9+273937: previous HI det at cz=9710.

HI 022632.1+274941: previous HI det at cz=9621.

HI 022741.1+271328: marginal detection corroborated by previous HI det at cz=5123.

HI 022742.7+261406: previous HI det at cz= 9504.

HI 022745.2+263507: previous HI det at cz=9789.

HI 022745.2+263507: merging system, tidal features.

HI 022751.5+275429: previously measured opt cz=10468.

HI 022816.3+261854: previous HI det at cz=5237.

HI 023052.0+261047: weak det, corroborated by previous HI det at cz=13289.

HI 023103.8+274053: previous HI det at cz=4587.

HI 023137.5+261010: previous HI det at cz=10869.

HI 023851.0+275109: previous HI det at cz=4587.

HI 024416.4+260648: opt id is galaxy in compact group HCG 020, at anomalous opt cz=10561 (other galaxies in group near 14500 km s^{-1}). Marginal det.

HI 024600.5+280145: previous HI det at cz=7954.

HI 024609.7+270247: previous HI det at cz=5728.

HI 024752.7+270607: U2272 at 024804.5+270609, detected at end of drift, 12s in RA off opt pos; opt pos not covered; tabulated flux is lower limit; det certain, but HI parms highly unreliable due to incomplete sampling of source region.

HI 025122.4+263459: previously measured cz=7485.

HI 033716.0+262357: large (30″) galaxy at (a) 033722.5+262505 and lesser one at (b) 033719.6+262255; due to exceptionally large HI centroid error, optical id tentatively assigned to (a), but remains ambiguous. Marginal det.

HI 040226.1+264950: previous HI det at cz=5639.

HI 040328.6+262149: previous HI det at cz=7064.

HI 041904.2+261210: previous HI det at cz=3751.

HI 042739.5+260545: high obscuration: near galactic plane; ambiguous opt id.

HI 060125.5+260524: Wein 163 at cz=5919; source region sparsely sampled; Dec centroid poorly constrained.

HI 060628.3+262314: previously measured cz=2717.

HI 062218.4+262631: optically invisible; high obscuration: ZOA.

HI 063840.8+263006: previously measured cz=9819.

HI 065004.2+262342: previously measured cz=9509.

Of the 166 HI detections, 62 coincide with previously known HI sources. Redshifts had been previously measured for an additional 18 galaxies, so that 52% of the redshifts reported here were previously unknown. Of the 166 objects detected, optical identifications are made with 115 previously cataloged galaxies, while 51 are previously unreported objects. Images of the HI detections' optical counterparts can be accessed through the aforementioned websites.

5. Quality of Inferred Parameters

In the final definition of the ALFALFA survey design and strategy that these precursor observations were meant to aid, evaluation of the useful quantities derived from the spectral dataset provided quantitative, albeit approximate, measures of survey strategy effectiveness. In this section, we use the precursor dataset to present a preliminary analysis of the parameters to be extracted from the ALFALFA survey dataset.

5.1. HI Positions

The accuracy of the positions of HI sources depends on (a) the pointing quality of ALFA and (b) our ability to accurately centroid on maps of HI emission. While the pointing characteristics of ALFA are still being evaluated, the average pointing errors for all ALFA beams — as estimated from bright sources of known positions — are smaller than $15''$. We evaluate the map centroiding component simply by propagating the uncertainties on flux integrals measured throughout the source map, and combining it in quadrature with a $10''$ rms pointing error. Estimated uncertainties on the HI centroids are tabulated in column 2 of Table 2. A histogram of the total HI centroid estimated errors is shown in Figure 2(a). The median on the HI centroid total estimated positional uncertainty is $36''$. In Figure 2(b), we plot the histogram of the positional difference between the HI centroid and the optical counterpart center. The median value of that difference is $34''$, suggesting that our positional error estimates are statistically correct.

5.2. Velocities and Widths

Figure 3 displays the difference between the systemic velocities measured respectively for the ALFA and for the LBW data, versus the systemic velocity itself. Figure 4 shows a comparison of the velocity widths measured on ALFA spectra with those measured on LBW spectra. Apart from a couple of objects with clearly underestimated errors, no significant difference between the two scales is seen. Note that the objects included in this comparison are among those with the lowest signal to noise in our sample (which is the reason why their initial detection needed corroboration).

Springob *et al.* (2005) have constructed a digital archive of some 9000 extragalactic HI spectra, the majority of which were obtained at Arecibo, centered on optically-identified galaxies, and have reprocessed the digital spectra to extract parameters using a homogeneous set of algorithms. Fifty–one of the detections presented in Table 2 are also represented in the optically-targeted HI archive; all of the archival spectra were obtained with one of the Arecibo dual polarization line feeds available before the Gregorian upgrade. A comparison of the velocity widths measured on ALFA spectra with those of previous HI observations given by Springob *et al.*, allows a comparison for high signal to noise sources. The correlation between reported and newly measured widths is

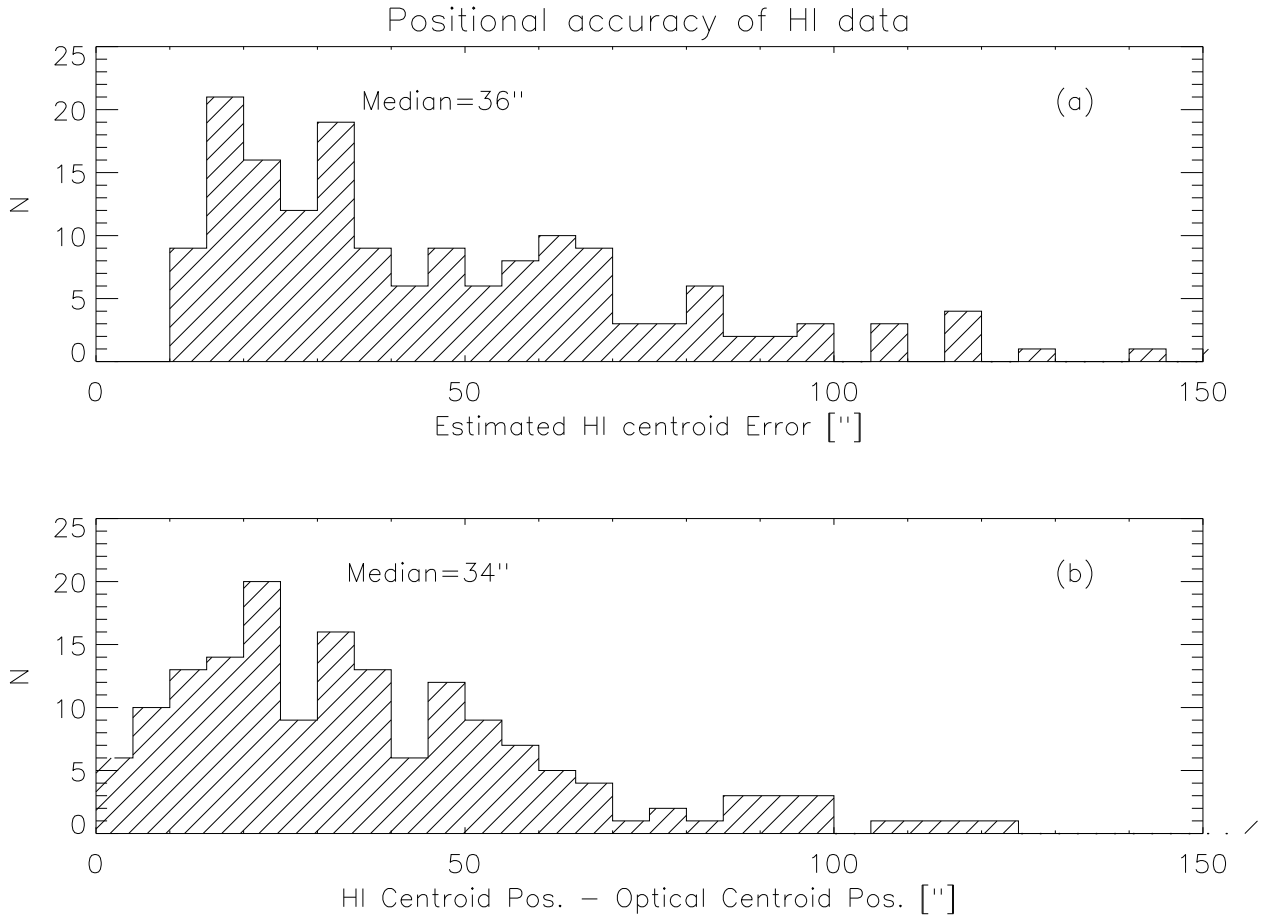

Fig. 2.— (a) Histogram of the estimated uncertainty on the HI centroid position, $(\epsilon_\alpha^2 + \epsilon_\delta^2)^{1/2}$, expressed in arcsec. (b) Histogram of the positional difference between the HI centroid and the center of the optical counterpart, in arcsec.

very good, guaranteeing the good quality of the extracted high signal to noise ALFA data and its immediate applicability in studies which may involve the luminosity–linewidth relation and other scaling relations.

5.3. HI Line Fluxes

In Figure 5, we compare the HI line flux integrals obtained from the single beam LBW spectra with those obtained from the composite spectra with ALFA. In spite of the large scatter, cross–calibration of the flux density scales appears satisfactory. Again, note that this subset of the data contains the objects closest to the detection limit of our survey. Possibly a more relevant comparison is that obtained for the objects with previously published HI flux integrals (Springob *et al.* 2005). Figure 6 shows such a comparison. In panel (a), we compare published flux integrals

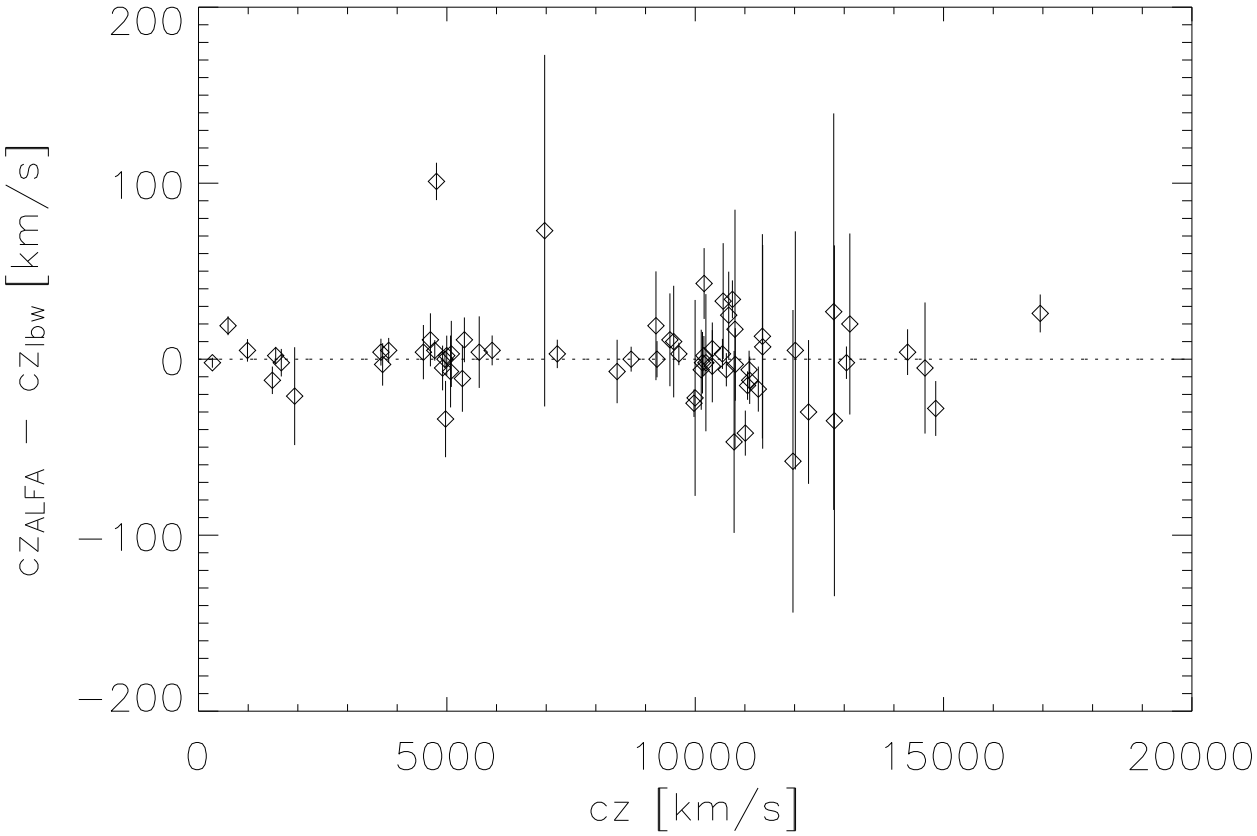

Fig. 3.— Systemic velocity difference between the ALFA and LBW spectra for 68 objects observed with both systems. Note that these objects are among the lowest signal–to–noise detections in the sample.

with those measured on the ALFA composite spectrum, which includes only the flux seen by a single beam, centered on the HI centroid position. The ALFA flux integrals fall slightly short of the published values, by about 15%. However, the published flux integrals, in their vast majority based on Arecibo single beam observations, have been corrected by a statistical dilution factor which takes into account the expected extent of the HI emission, based on the optical size of the galaxy. In panel (b) of Figure 6, for those objects for which a significant indication of extended HI emission is available, we use the ALFA flux integrals F_m, which better represent the total flux integral. We exclude from the comparison HI 014729.9+271958 (IC 1727) and HI 014753.9+272555 (NGC 672): the emission of the two galaxies is blended and a detailed analysis of the system is required to produce accurate estimates of the respective fluxes, a task beyond the scope of this preliminary report. Figure 6 (a) and (b) indicate that the recovery of HI flux integrals via ALFA is largely consistent with well established previous efforts.

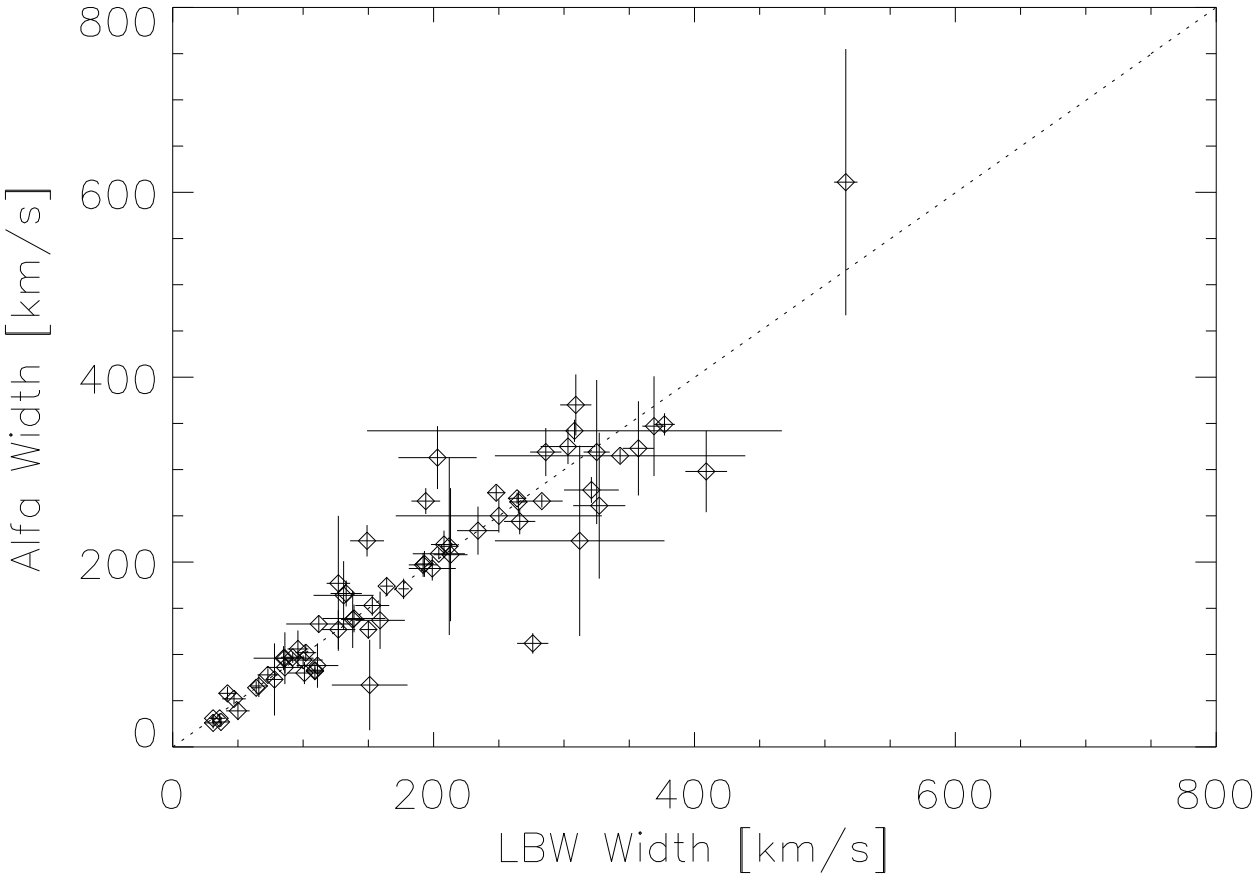

Fig. 4.— Comparison of velocity widths as measured in the ALFA and LBW spectra for 68 objects observed with both systems. The diagonal line of slope 1 is shown as a visual aid. Note that these objects are among the lowest signal–to–noise detections in the sample.

5.4. Distances

Source distances D_{pec}, as listed in Column 6 of Table 4, are obtained from the peculiar velocity model of the local Universe of Tonry *et al.* (2000). The model provides the expected peculiar velocity at a given point in space, and it can be inverted to yield the distance to a galaxy of given angular coordinates and observed redshift. We have used D_{pec} to compute the HI mass in Column 7 of Table 4. A word of caution is however needed. The inversion of the peculiar velocity model yields single–valued solutions throughout the region populated by sources in Table 4 (unlike, for example, of what would take place in the direction of the Virgo cluster). Throughout this region, the dipole component of the peculiar velocity is negative. This component does not vanish at large distances, and beyond 60 Mpc D_{cmb} probably yields a more accurate estimate of distance. Between $D_{cmb} = 40$ to 60 Mpc, an average between D_{cmb} and D_{pec} may be a better estimate of distance, although we note that the differences between the two values are small.

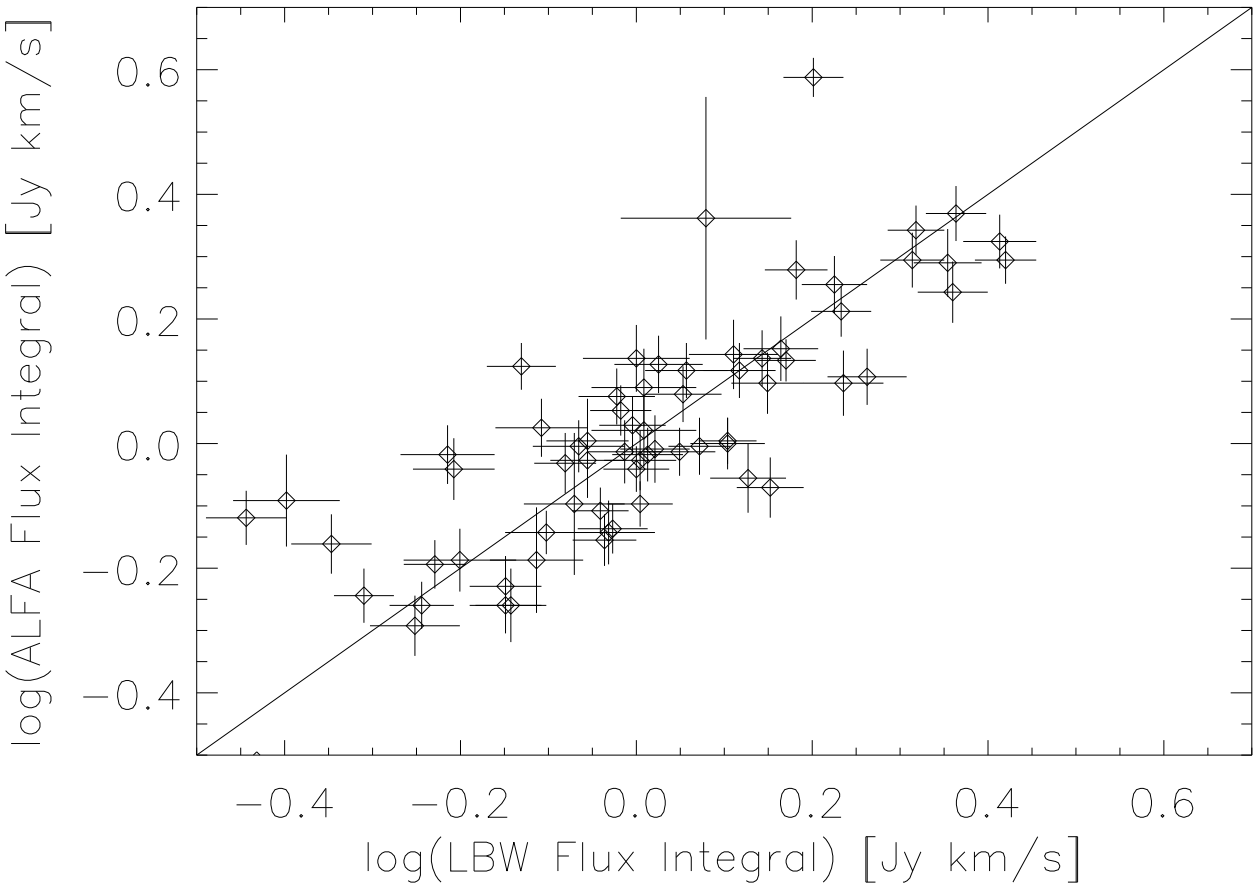

Fig. 5.— Comparison of HI line flux integrals F_c as measured in the ALFA and LBW spectra for 68 objects observed with both systems. The diagonal line of slope 1 is shown as a visual aid. Note that these objects are among the lowest signal–to–noise detections in the sample.

The adoption of such a peculiar velocity model yields, for nearby galaxies in the part of the sky sampled by this study, significantly larger estimates of distance than those obtained assuming a pure Hubble flow model, D_{cmb}. For example, for the 7 objects with $D_{cmb} < 10$ Mpc, the mean D_{pec} is about 6 Mpc larger than D_{cmb}. For those, the assumption of pure Hubble flow would yield distances which are smaller by more than a factor of 4 and HI masses that are smaller by more than a factor of 20, than if a peculiar velocity flow model is assumed. In addition to large–scale flows, the peculiar velocity model includes a 'thermal' component of 187 km s^{-1}, which translates in an additional distance uncertainty of 2.7 Mpc. This illustrates how the assumption of a distance model can have an important effect in the derivation of the HI mass function, as its low mass slope is strongly dependent on the parameters of (few known) nearby objects (Masters, Haynes & Giovanelli 2004).

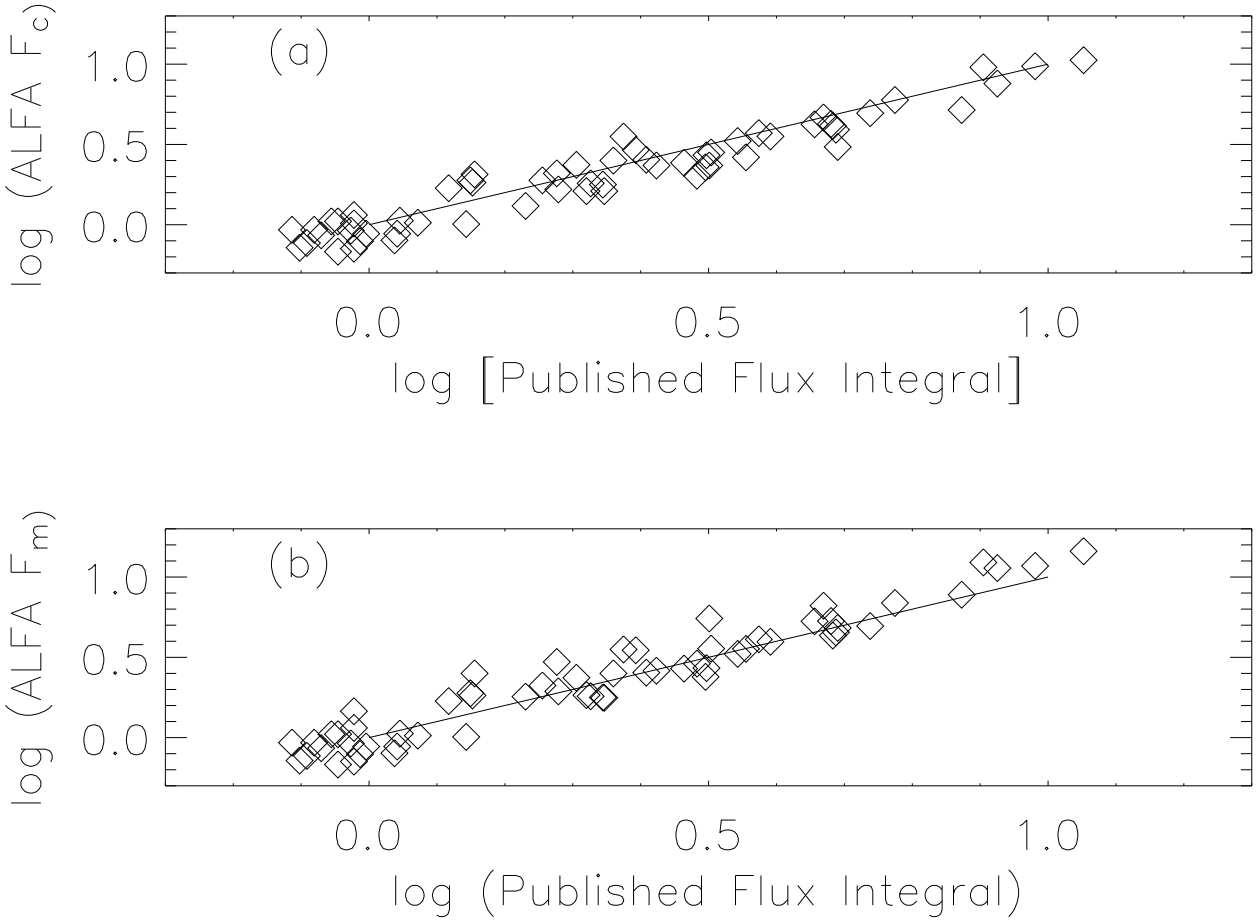

Fig. 6.— (a) Comparison of HI flux integrals F_c, as measured in the ALFA composite spectra, with those available from the literature. F_c are uncorrected for beam dilution. (b) Comparison of HI line flux integrals F_m, obtained by integrating ALFA maps of the sources, with those obtained from the literature. The diagonal lines of slope 1 are shown as visual aids.

6. Survey Sensitivity

While the sky coverage of the precursor observations was uneven and the sampling density of some of the regions covered was poor (given the vagaries forced by the telescope schedule), the data obtained lend themselves to a preliminary appraisal of the sensitivity limits of the ALFALFA survey. As discussed in Paper I, a 2–pass drift survey, i.e. one with drift tracks spaced about $1'$ in Declination, yields an effective integration time per beam area of ∼48 sec, or a map with effective integration per pixel area of 30 seconds, if no significant deterioration of the spatial resolution is imposed. The signal extraction from the precursor observations was however exercised on single beam drift tracks, which have an rms of $3.5 \times (res/10)^{-1/2}$ mJy, where res is the spectral resolution of the data after smoothing, in km s^{-1}. The detection threshold of a given spectral feature depends

on the width of the feature, as discussed in Paper I, so that spectral smoothing can be increased for a broad feature, and the rms noise accordingly decreased. This approach remains valid until a threshold width is reached, beyond which further smoothing is overcome by the effect of large–scale instabilities in the spectral baseline, which cannot be undone by smoothing. In Paper I we assumed that the threshold width for our data lies in the vicinity of 200 km s^{-1}.

Figure 7 displays a plot of the HI line flux integral of the HI detections in our precursor run, versus their velocity widths. The figure corroborates the expectation that the sensitivity limit of the survey depends on velocity width, lower flux integrals being detectable at smaller widths. The dashed lines inset in the figure represent possible detection thresholds at different levels of signal–to–noise. Suppose the detection threshold is defined as

$$F_{th} = (S/N) \times (rms) \times W \tag{1}$$

where S/N is a signal–to–noise fiducial figure for detection and rms is the root mean square noise over a pixel, after smoothing of the spectrum. With the noise rms expressed in Jy and the width in km s^{-1}, the flux integral F_{th} is in Jy km s^{-1}. If the spectrum is smoothed to a resolution equal to $W/2$ for $W < 200$ km s^{-1}, and to a resolution equal to 200/2 km s^{-1} for $W \geq 200$ km s^{-1}, then for the rms appropriate to single drift maps (cf. Paper I)

$$F_{th} = \begin{cases} 0.22\ (S/N)\ (W/200)^{1/2} & \text{if } W < 200 \\ 0.22\ (S/N)\ (W/200) & \text{if } W \geq 200 \end{cases} \tag{2}$$

The dashed lines in Figure 7 are Eqn. 2 for nominal figures of S/N 4, 5 and 6, which show that we are able to detect sources with flux well below the nominal sensitivity limit for a conservative signal–to–noise ratio of 6, as discussed in Paper I. A few sources of large width are detected at signal–to–noise levels even significantly lower than 4. This can be attributed to the fact that extragalactic line profiles are not boxlike, but rather two–horned: a spectral feature of $W = 300$ km s^{-1}, which consists of two horns each 35 km s^{-1} wide, can be detected with similar ease to that with which we can detect a 300 km s^{-1} boxlike spectral line with twice the flux integral. Figure 7 can be used to illustrate two important points:

- The spatially two–dimensional data cubes that will be produced by ALFALFA will have a sensitivity per pixel 1.5 times better than the single drift, position–velocity maps used to obtain candidate detections in the precursor run; thus a conservative threshold of $S/N = 6$ for the ALFALFA survey is equivalent to the dashed line of $S/N = 4$ in Figure 7. To that level, we expect the vast majority of ALFALFA candidate detections will not need follow–up corroborating observations.

- ALFALFA candidate detections to $S/N \geq 4$ will deliver a substantial additional fraction of confirmations, with modest amount of follow–up telescope time, as discussed in Section 7 of Paper I.

Figure 8 shows the distribution of HI mass plotted as a function of source distance. The dotted lines in Figure 8 correspond to flux density integrals of 1. and 0.72 Jy km s^{-1}. The lower level corresponds to the 5σ limit for a $W = 200$ km s^{-1} source with an effective integration of 30 seconds per map pixel, which will apply to the ALFALFA survey. The dashed line corresponds to a flux density of 5.6 Jy km s^{-1}, the 5σ detection limit for a $W = 200$ km s^{-1} source in the HIPASS survey, as obtained by the same rationale as that by which our limits are estimated. It is apparent that, of the 166 objects detected by our experiment, HIPASS would have detected 10% or fewer, and none of those farther than 100 Mpc.

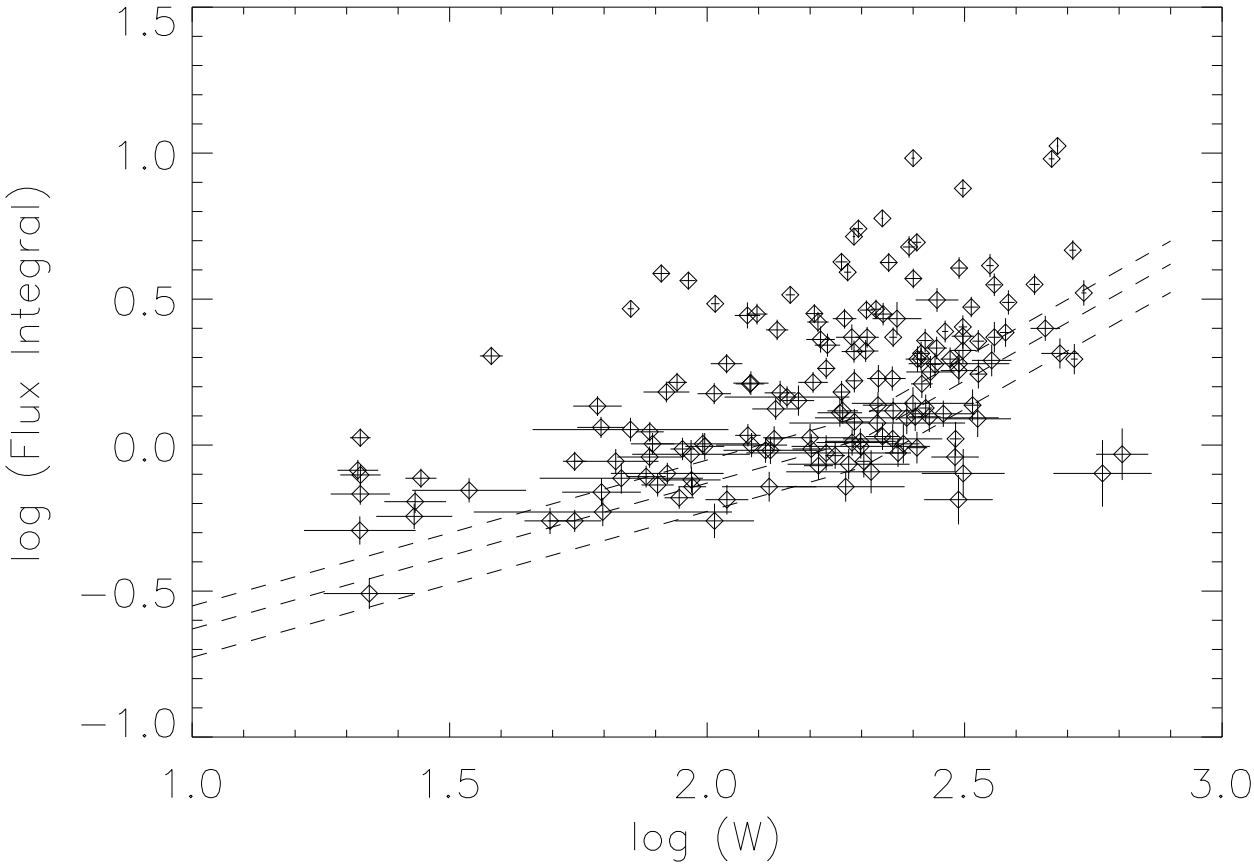

Fig. 7.— HI flux integral plotted versus velocity width, for the detected sample. The three dashed lines correspond to the flux threshold F_{th} one obtains for a signal–to–noise ratio of, respectively, 4, 5 and 6, using Eqn. 2.

7. Discussion

The call for precursor observations by NAIC during the period of ALFA commissioning was intended to provide potential ALFA survey teams with the opportunity to gain experience with the

system on the earliest possible timescale, and to contribute to the commissioning effort through debugging and testing of telescope control and data taking hardware and software. From our perspective, this "shared-risk" collaboration has proved very advantageous: both the ALFALFA survey and the ALFA system are better as a result.

While most of the data obtained during our precursor observations were not of science quality, we nonetheless are greatly encouraged both by the detection rate achieved in the precursor run and the nature of the extragalactic HI sources presented here in Table 2. After less than 1% of the planned full survey time and under less-than-optimal conditions, we can clearly see the delivery of ALFALFA's science promise.

Even without a correction for incompleteness, the redshift distribution of the detected sources carries clear signature of the large scale structure in the distribution of galaxies in the Local Universe. Two strong peaks occur near 70 and 150 Mpc, as expected given that the region surveyed overlaps the Perseus–Pisces Supercluster. For the same reason, the number of sources nearer than 50 Mpc is much smaller than would be expected for a random sample, because a prominently underdense void separates the Local Group from Pisces-Perseus. Because of the extreme environmental conditions represented by the regions sampled, the set of detected sources presented here does not lend itself to reliable inferences regarding the HI mass function. As discussed in Paper I, the determination of the HI mass function in a variety of environments is a main science objective of ALFALFA.

As illustrated in Figure 8, ALFALFA will survey the HI universe to a distance of 250 Mpc, allowing detection of massive HI rich objects. The HI detection with the highest redshift found in the precursor observations, HI 020329.8+273909, is identified with a very blue galaxy, found in the KISO survey with previously unknown redshift, near $cz = 17,000$ km s^{-1}, which places the HI line close to the edge of our bandpass. The source with the highest HI mass, HI 020248.2+263434, is identified with the previously cataloged galaxy UGC 1533, a barred spiral seen nearly face–on at a distance of 208 Mpc ($cz_\odot = 14,600$ km s^{-1}). Its HI mass, 5×10^{10} $M_\odot$, is about one order of magnitude larger than that of the Milky Way.

As discussed in detail in Paper I, for a HI survey conducted with a high sensitivity telescope like Arecibo, the probability of maximizing detection of the lowest mass objects is enhanced more by increasing the solid angle coverage than by increasing the survey depth. Indeed, these precursor observations have already detected three objects with HI masses lower than 10^7 $M_\odot$, all located within 10 Mpc from us. Given the model we have used for the peculiar velocity field, no object in our detected sample was assigned a distance smaller than 5.5 Mpc. Note that the "thermal" rms peculiar velocity of galaxies translates into a distance uncertainty of about 2.7 Mpc, and thus the distances of the nearest objects are highly uncertain. These objects belong to the group of which the brightest members are NGC 672 (HI 014753.9+272555) and IC1727 (HI 014729.9+271958). We detected 8 possible members of the group, namely: HI 014105.8+272007, HI 014214.9+262202, HI 014441.4+271707, HI 014640.9+264754, HI 014729.9+271958, HI 014753.9+272555, HI 015519.2+275645, HI 021404.3+275302.

Given the vicinity and abundance of gas–rich systems and the availability of primary distances for several group members (7.9 Mpc for NGC 672, 5.4 Mpc for UGC 1281, 4.7 Mpc for AGC111977=KK16 and for AGC111164=KK17 and 5.0 Mpc for NGC 784), a detailed study of this group appears as potentially very rewarding and will follow.

Albeit at very small distances, the detected objects with the lowest HI masses have small sizes, unresolved by the telescope beam, so that their diameters are less than a few kpc. They are associated with very low surface brightness optical counterparts, with optical diameters on the order of 1 kpc. The velocity widths of these systems tend to be quite small, on the order of 25 km s^{-1}, and their halo masses may well be less than 10^8 $M_\odot$. The determination of the cosmic density of low mass, optically faint gas-rich dwarfs constitutes one of the main goals of ALFALFA.

The procedure for source identification which yielded the 166 detections presented here was biased against narrow–line, small angular size sources. Because of the unusually large amount of RFI with similar characteristics in these early ALFA data, we did not seek detection confirmation of most narrow-width candidates. Since much of the narrow RFI, especially at frequencies near 1420 MHz, was internally generated and has since been eliminated, the prospects for detecting narrow line HI signals has considerably improved since these early ALFA observations. For that reason, and because the local volume probed by these observations is significantly underdense relative to other regions of the ALFALFA sky, we expect the overall detection rate of low mass objects to be considerably higher than that of the current sample. In fact, as discussed in greater detail in Paper I, we can confidently predict that the full ALFALFA survey covering more than 7000 deg^2 will detect more than 100 times as many HI sources as reported here. We look forward to the surprising objects among them.

RG and MPH acknowledge the partial support of NAIC as Visiting Scientists during the period of this work. GLH acknowledges travel support from NAIC. This work has been supported by NSF grants AST–0307661, AST–0302049, AST–0435697, AST–0347929, AST–0407011; DGICT of Spain grant AYA2003–07468–C03–01; RFBR grant 04-02-16115; and by a Brinson Foundation grant. We thank Robert Brown, the Director of NAIC, for stimulating the development of major ALFA surveys, Jeff Hagen and Mikael Lerner for numerous last minute fixes to CIMA, and Hector Hernandez for a sensible approach to telescope scheduling.

REFERENCES

Barnes, D.G, Staveley–Smith, L., de Blok, W.J.G., Oosterloo, T. Stewart, I.M. *et al.* 2001, MNRAS, 322, 486

Giovanelli, R. *et al.* 2005, AJ, submitted (Paper I)

Kildal, P.S., Baker, L., Hagfors, T. & Giovanelli, R. 1993, IEEE Trans. Anten. Propag. 41, 1019

Lang, R.H., Boyce, P.J., Kilborn, V.A., Minchin, R.F., Disney, M.J. *et al.* 2003, MNRAS, 342, 738

Masters, K.L., Haynes, M.P. & Giovanelli, R. 2004, ApJ 607, L115

Masters, K.L. 2005, Ph.D. Thesis, Cornell University

Meyer, M.J., Zwaan, M.A., Webster, R.L. *et al.* 2004, MNRAS, 350, 1195

Nilson, P. 1973, *Uppsala General catalog fo Galaxies*, Royal Soc. of Sciences of Uppsala, ser. V:A. vol. 1

Rosenberg, J. L. & Schneider, S. E. 2000, ApJS, 130, 177

Springob, C.M., Haynes, M.P., Giovanelli, R. & Kent, B.R. 2005, ApJS, in press.

Tonry, J.L., Blakeslee, J.P., Ajhar, E.A. & Dressler, A. 2000, ApJ, 530, 625

Zwaan, M., Briggs, F. H., Sprayberry, D. & Sorar, E. 1997, ApJ, 490, 173

Zwaan, M.A., Meyer, M.J., Webster, R.L., Staveley–Smith, L., Drinkwater, M.J. *et al.* 2004, MNRAS, 350, 1210

Table 1. Precursor Run Statistics

Description	Number
ALFA Candidate Detections	730
Candidates reobserved with LBW	165
Detections confirmed by LBW	68
ALFA internally corroborated	98
Total confirmed Detections	166
N with very likely optical counterparts	162
N with previous HI detections	62
N with previously known redshifts	80
N with previously cataloged photometry	115

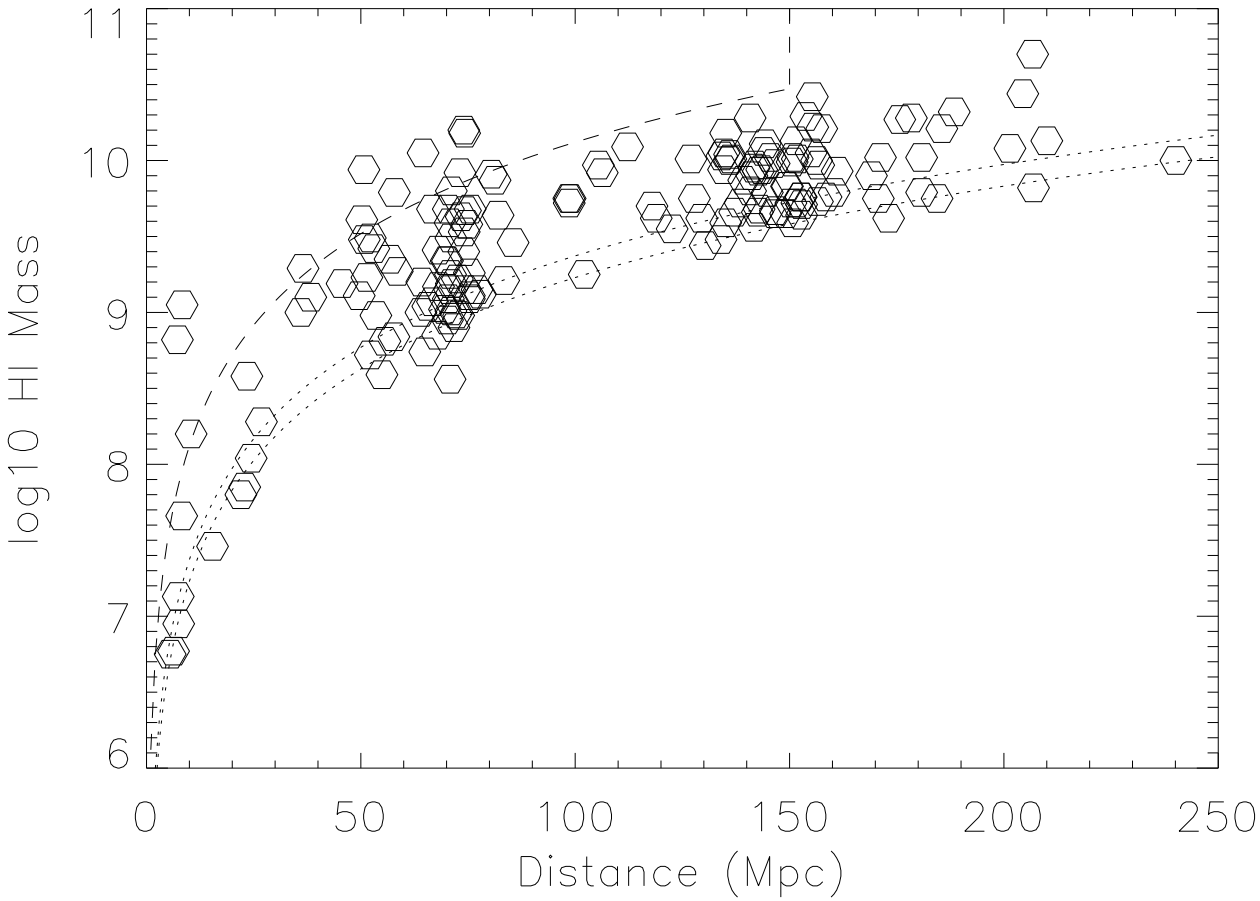

Fig. 8.— Distribution of HI Mass as a function of distance, for the detected sample. Distances are estimated from a peculiar velocity model of the Local Universe. The net effect of this model, for galaxies in this part of the sky, is that distance estimates are significantly larger than those that would be obtained from a pure Hubble flow model. The highest of the two dotted lines corresponds to a flux integral of 1.0 Jy km s^{-1}; the lower dotted line corresponds to 0.72 Jy km s^{-1}, the 5–sigma limit for a $W = 200$ km s^{-1} source with an effective integration of 30 seconds per map pixel, which will apply to the ALFALFA survey. The dashed line corresponds to a flux integral of 5.6 Jy km s^{-1}, which corresponds to the HIPASS 5σ detection limit for a $W = 200$ km s^{-1} source.

Table 2. Parameters of ALFA Detections

Source	$\epsilon_\alpha, \epsilon_\delta$ sec, "	$cz_\odot(\epsilon_{cz})$ km s^{-1}	$W(\epsilon_w)$ km s^{-1}	rms mJy	$F_c(\epsilon_f)$ Jy km s^{-1}	F_m Jy km s^{-1}	Notes
HI 001709.7+271616	4.2, 28	3707(8, 0)	150(11)	3.10	1.42(0.18)		L *
HI 002115.8+262318	2.3, 27	9210(7,25)	158(37)	2.02	1.06(0.12)		L *
HI 002312.5+272644	1.5, 20	3940(8, 0)	192(11)	2.30	2.09(0.19)	2.96	*
HI 002818.8+272136	4.7, 62	9611(8, 0)	361(11)	2.27	3.54(0.33)		*
HI 002905.0+272936	4.7, 25	8710(5, 0)	78(8)	2.00	1.01(0.09)		L *
HI 003027.1+263852	3.2, 31	9671(4, 0)	260(6)	1.81	1.97(0.18)	2.49	L
HI 003052.6+272328	3.5, 43	11270(10, 0)	159(14)	1.92	0.97(0.12)		L
HI 003831.2+262132	1.3, 16	7223(4, 0)	93(6)	1.43	0.72(0.06)		L
HI 003855.1+265753	0.8, 11	5178(5, 0)	193(7)	2.11	1.66(0.16)	1.94	*
HI 004034.8+270239	0.9, 13	5134(4, 0)	124(6)	3.26	2.81(0.24)	3.38	*
HI 004113.4+272248	2.4, 31	10344(14, 0)	313(19)	1.71	2.11(0.22)		L
HI 004256.8+271522	1.0, 13	5292(7, 0)	219(10)	2.63	2.81(0.26)	3.57	*
HI 004357.1+260731	2.1, 57	4905(1, 0)	27(2)	1.90	0.77(0.06)		*
HI 004404.2+261243	1.5, 18	10088(6, 0)	516(8)	1.65	1.97(0.25)		*
HI 004411.5+265042	0.7, 10	5197(1, 0)	251(2)	1.81	9.61(0.68)	11.73	
HI 004456.0+272758	1.6, 37	5205(5, 0)	119(7)	1.85	1.08(0.10)		*
HI 004629.4+264134	2.3, 31	5089(9, 0)	93(13)	1.61	0.76(0.08)		L
HI 004645.5+275553		6969(3,84)		1.77	2.30(1.30)		L *
HI 004650.7+262846	0.9, 13	4961(3, 0)	229(4)	1.63	2.34(0.19)	2.61	*
HI 004716.1+274854	2.5, 32	4748(11, 0)	313(16)	1.88	2.36(0.24)		*
HI 004738.1+264856	1.1, 16	4956(5, 0)	103(8)	1.83	1.50(0.13)		
HI 004803.3+273717	1.7, 23	4955(5, 0)	538(6)	1.99	3.32(0.35)		*
HI 004816.9+262806	1.8, 23	5270(6, 0)	177(8)	1.63	0.92(0.10)		*
HI 004834.5+274100	0.9, 19	5216(4, 0)	161(6)	2.00	2.82(0.22)	3.58	*
HI 005009.5+271328	1.2, 16	4925(4, 0)	134(5)	2.07	1.05(0.11)		*
HI 005124.7+271517	2.9, 39	4527(9,11)	103(20)	2.11	0.55(0.08)		L
HI 005305.3+272909	1.2, 16	4756(5, 0)	61(7)	1.84	1.36(0.11)		L *
HI 010032.5+270540	2.1, 31	11008(10, 0)	256(14)	2.36	1.97(0.21)		L
HI 010158.0+263010	2.8, 38	10065(21, 0)	68(30)	1.38	0.77(0.10)		*
HI 010225.7+263713	1.6, 23	4973(5,18)	229(26)	1.74	1.31(0.14)		L *
HI 010318.1+264747	0.9, 12	5074(11, 0)	135(15)	1.69	1.33(0.12)		L *
HI 010456.8+264942	1.0, 14	14275(5, 0)	253(7)	1.85	1.25(0.15)		L
HI 010654.5+263054	1.8, 22	10147(15, 0)	121(21)	1.56	1.00(0.10)		L
HI 010703.4+271516	0.9, 12	10121(9,20)	132(31)	1.82	0.96(0.11)		L
HI 011302.6+273832	1.6, 18	4961(3, 0)	22(5)	1.74	0.31(0.04)		L *
HI 011443.5+270813	0.8, 10	3625(1, 0)	103(2)	2.04	3.05(0.22)	4.82	*
HI 011643.2+265307	3.7, 58	12282(8,34)	62(49)	1.83	0.59(0.07)		L
HI 011743.9+270006	0.7, 11	12148(7, 0)	138(10)	2.36	1.51(0.15)		*
HI 012242.5+265157	0.9, 14	9064(7,32)	142(46)	1.58	1.46(0.13)		*
HI 012403.9+270300	0.6, 10	4923(7, 0)	156(10)	1.83	1.89(0.16)		*
HI 012405.2+280433	0.9, 60	4084(8, 0)	166(11)	4.08	2.30(0.25)		*
HI 012607.5+275810	1.3, 17	4031(10, 0)	66(14)	1.91	0.88(0.09)		*
HI 012944.1+272249	0.7, 10	12646(8, 0)	160(11)	1.70	1.64(0.14)	2.55	*
HI 013152.5+271912	1.5, 22	3828(5, 0)	55(7)	1.75	0.55(0.05)		L
HI 013315.1+261438	0.7, 10	6960(3, 0)	289(4)	1.90	2.45(0.22)		
HI 013339.0+262439	1.1, 16	11096(10, 0)	234(14)	1.27	0.94(0.11)		L
HI 013716.0+262606	1.2, 17	3880(2, 0)	55(3)	1.62	0.88(0.07)		*
HI 013740.2+271042	0.8, 11	11085(9, 0)	336(12)	1.68	1.75(0.21)		L

Table 2—Continued

Source	$\epsilon_\alpha, \epsilon_\delta$ sec, "	$cz_\odot(\epsilon_{cz})$ km s^{-1}	$W(\epsilon_w)$ km s^{-1}	rms mJy	$F_c(\epsilon_f)$ Jy km s^{-1}	F_m Jy km s^{-1}	Notes
HI 014105.8+272007	1.3, 18	280(2, 0)	27(4)	2.03	0.64(0.06)		L *
HI 014147.3+273159	5.3, 85	10830(9,39)	229(57)	1.69	1.05(0.13)		*
HI 014214.9+262202	1.7, 23	364(1, 0)	21(1)	1.82	1.06(0.08)		*
HI 014331.2+275930	3.2, 39	10179(18, 0)	308(26)	1.67	1.80(0.20)		L
HI 014428.3+275522	0.7, 9	4048(1, 0)	192(1)	1.85	5.18(0.38)	7.76	*
HI 014441.4+271707	0.7, 10	430(2, 0)	38(2)	1.82	2.02(0.15)	2.89	*
HI 014455.3+272942	4.3, 57	12802(10,99)	585(144)	1.55	0.80(0.24)		L *
HI 014640.9+264754	2.3, 31	370(2, 0)	21(3)	2.09	0.68(0.06)		*
HI 014653.7+280448	2.0, 60	3597(19, 0)	233(27)	3.90	2.71(0.38)		*
HI 014724.3+275312	1.6, 22	3707(7, 0)	432(10)	1.76	3.55(0.31)	3.95	*
HI 014729.9+271958		351(2, 0)	117(3)	1.88	54.39(3.81)		*
HI 014753.9+272555		436(2, 0)	175(3)	1.77	69.25(4.85)		*
HI 014837.9+273259	2.1, 28	11017(8, 0)	384(11)	2.10	3.08(0.31)	2.92	*
HI 014915.3+274248	2.6, 32	10760(9, 0)	261(13)	1.91	1.62(0.19)	1.90	*
HI 015011.6+271145	0.7, 10	3511(1, 0)	218(1)	1.69	5.98(0.43)	6.89	*
HI 015013.0+273842	0.7, 9	3543(1, 0)	479(2)	1.81	10.58(0.77)	14.47	*
HI 015047.7+271714	2.7, 34	14627(9,35)	307(51)	1.54	0.65(0.14)		L
HI 015150.7+274448	1.7, 22	10749(4, 0)	89(5)	2.06	0.97(0.09)		L
HI 015439.1+274824	1.2, 15	14842(9, 0)	183(13)	1.81	1.31(0.14)		L
HI 015439.8+271111	1.0, 15	8428(10, 0)	270(14)	1.75	1.25(0.16)		L *
HI 015519.2+275645	1.0, 13	219(1, 0)	21(2)	2.11	0.79(0.07)		*
HI 015536.6+274154	2.3, 34	8356(6, 0)	83(9)	1.71	1.52(0.13)		
HI 015751.8+264537	1.6, 22	12435(9, 0)	279(13)	1.83	2.15(0.20)	2.54	
HI 015857.7+265710	1.9, 25	13044(7, 0)	34(10)	1.68	0.70(0.07)		L
HI 015917.6+270027	1.9, 24	5313(6, 0)	129(9)	1.95	0.96(0.10)		L *
HI 015937.0+272555	1.2, 14	5276(4, 0)	203(6)	1.79	2.90(0.23)		*
HI 015952.5+262407	1.0, 14	5226(6, 0)	109(8)	1.57	1.90(0.15)	2.60	*
HI 020133.9+262914	0.8, 11	5155(6, 0)	512(8)	1.54	4.65(0.38)	6.63	*
HI 020144.4+263227	0.8, 12	5014(4, 0)	182(5)	1.69	4.24(0.32)	5.32	*
HI 020248.2+263434	0.8, 11	14603(7, 0)	204(11)	1.91	2.34(0.20)	5.02	*
HI 020304.8+271222	3.0, 52	4790(7, 0)	109(11)	1.82	0.65(0.08)		L *
HI 020329.8+273909	2.9, 38	16946(4, 0)	80(6)	2.01	0.73(0.07)		L *
HI 020343.0+261608	2.5, 36	5009(11,40)	188(59)	1.55	0.86(0.11)		*
HI 020353.5+261719	1.9, 22	5060(4, 0)	88(6)	1.55	0.66(0.06)		*
HI 020430.7+275454	0.8, 12	4710(2, 0)	187(3)	1.69	3.91(0.29)	4.53	*
HI 020530.0+272806	5.5, 65	11968(9,72)	213(103)	1.58	1.19(0.13)		L
HI 020558.3+272121	1.5, 18	4939(5, 0)	182(7)	1.92	1.52(0.14)	1.88	
HI 020626.5+270152	1.1, 19	4974(6, 0)	251(9)	1.86	3.72(0.30)	4.09	*
HI 020902.1+273202	1.2, 19	9868(6, 0)	121(8)	1.60	1.62(0.13)		*
HI 020913.9+264536	3.1, 41	12788(9, 0)	327(12)	1.95	1.37(0.18)		L *
HI 020954.1+273147	1.4, 23	4914(9, 0)	77(12)	1.61	0.91(0.08)		L *
HI 021309.0+274650	2.0, 29	13113(8,50)	198(72)	1.65	0.99(0.10)	2.02	L
HI 021328.9+263102	1.4, 20	14436(9, 0)	296(13)	1.63	1.97(0.19)	2.78	
HI 021404.3+275302	0.8, 12	594(2, 0)	81(3)	1.91	3.87(0.29)	6.28	L *
HI 021510.4+262415	1.9, 27	4998(9, 0)	193(13)	1.63	1.20(0.13)		L
HI 021640.8+260835	3.7, 58	11352(13, 0)	240(18)	2.20	1.01(0.17)		L
HI 022102.1+274615	4.0, 53	9539(5, 0)	164(8)	2.11	2.64(0.22)		*
HI 022103.9+270204	2.9, 38	10800(6, 0)	303(8)	1.74	1.05(0.15)		L *

Table 2—Continued

Source	$\epsilon_\alpha, \epsilon_\delta$ sec, "	$cz_\odot(\epsilon_{cz})$ km s^{-1}	$W(\epsilon_w)$ km s^{-1}	rms mJy	$F_c(\epsilon_f)$ Jy km s^{-1}	F_m Jy km s^{-1}	Notes
HI 022138.2+280302	4.2, 48	10674(8,22)	356(33)	2.29	1.95(0.26)		L
HI 022224.8+262552	1.4, 20	11143(6, 0)	336(9)	1.51	2.27(0.21)	2.76	*
HI 022335.8+271851	3.8, 53	10662(3,39)	185(56)	1.59	0.72(0.09)		*
HI 022340.2+270927	1.7, 24	10660(5, 0)	170(7)	1.67	1.83(0.16)		*
HI 022345.8+262214	5.4, 83	9566(9,22)	302(34)	1.54	0.91(0.11)		L
HI 022348.9+272848	7.0, 98	10718(10,19)	453(31)	1.64	2.51(0.26)		*
HI 022355.8+270618	2.3, 30	5474(5,19)	98(28)	1.85	1.01(0.09)		*
HI 022405.6+263900	1.5, 21	9230(9, 0)	62(12)	2.22	0.69(0.08)		L *
HI 022459.4+260314	4.0, 75	10099(4,22)	271(31)	3.02	1.78(0.24)		*
HI 022533.4+264458	2.7, 39	10363(5, 0)	277(7)	1.73	1.89(0.18)		*
HI 022538.8+271709	1.1, 23	8997(7, 0)	184(10)	1.69	2.71(0.22)		*
HI 022542.3+265853	3.2, 42	9976(6, 0)	265(8)	1.71	1.34(0.15)		L
HI 022558.5+271607	1.0, 15	10215(5,38)	335(54)	1.96	1.23(0.19)	2.65	L *
HI 022609.4+273549	3.3, 46	9995(10, 0)	228(14)	1.92	1.69(0.17)		*
HI 022617.1+260750	4.1, 63	10250(9,87)	244(124)	2.31	1.24(0.17)		*
HI 022620.2+271315	5.5, 96	10384(9,55)	639(79)	1.52	0.93(0.21)		*
HI 022629.9+273937	5.7, 63	9717(7,22)	191(33)	1.59	1.02(0.11)		*
HI 022632.1+274941	3.4, 52	9632(6, 0)	265(8)	2.00	2.28(0.22)		*
HI 022740.9+265524	2.9, 43	10548(8, 0)	164(11)	1.82	0.85(0.10)		L
HI 022741.1+271328	2.5, 47	5125(12,45)	314(64)	1.69	0.80(0.17)		*
HI 022742.7+261406	3.5, 62	9505(5, 0)	313(6)	1.85	2.54(0.24)		*
HI 022745.2+263507	1.6, 24	9806(5, 0)	62(7)	1.84	1.15(0.10)		*
HI 022751.5+275429	2.7, 34	10562(8,30)	287(44)	1.55	1.28(0.14)		L *
HI 022816.3+261854	0.7, 11	5249(4, 0)	466(6)	1.65	9.56(0.70)	12.33	*
HI 022850.0+264500	1.6, 23	9529(6, 0)	260(9)	1.99	2.06(0.20)		
HI 022900.2+263041	4.2, 68	9490(10,20)	131(31)	1.75	0.72(0.09)		L
HI 022901.5+260509	1.7, 20	5912(6, 0)	98(9)	2.65	0.99(0.11)		L
HI 022919.3+272107	1.7, 25	1553(4, 0)	26(5)	2.43	0.57(0.06)		L
HI 023023.1+275653	1.6, 25	4746(4, 0)	77(5)	2.00	1.11(0.09)		
HI 023052.0+261047	2.5, 40	13300(10,28)	484(42)	1.62	2.06(0.26)	2.51	*
HI 023058.9+275709	0.8, 11	1596(1, 0)	71(1)	2.13	2.93(0.21)		
HI 023103.8+274053	3.9, 75	4549(5,24)	198(34)	1.59	1.03(0.11)		*
HI 023121.5+261239	3.1, 49	2523(2, 0)	145(3)	1.87	3.27(0.24)		
HI 023124.6+264706	1.0, 14	10979(7, 0)	325(10)	1.63	2.97(0.25)	4.67	
HI 023133.0+264727	0.8, 12	4559(3, 0)	87(4)	1.71	1.64(0.13)		
HI 023135.9+263155	1.5, 23	3701(1, 0)	20(2)	1.94	0.82(0.07)		
HI 023137.5+261010	1.1, 15	10874(4, 0)	212(5)	1.89	2.92(0.23)	3.50	*
HI 023138.9+271130	2.6, 45	985(4, 0)	21(6)	2.87	0.51(0.06)		L
HI 023203.1+261156	1.8, 25	10807(4,17)	83(24)	1.77	0.80(0.07)		L
HI 023234.8+275608	3.0, 37	4668(5,11)	219(17)	1.73	1.07(0.12)		L
HI 023325.2+271204	3.2, 44	5352(7, 8)	214(15)	2.04	1.37(0.15)		L
HI 023329.2+270136	2.2, 35	1666(5, 0)	76(7)	1.90	0.78(0.07)		L
HI 023516.3+280108	0.7, 12	2705(2, 0)	91(3)	2.67	3.66(0.27)		
HI 023851.0+275109	0.7, 10	4595(3, 0)	313(4)	2.71	7.57(0.58)	11.37	*
HI 024055.2+264046	4.0, 75	1487(5, 0)	49(6)	2.30	0.55(0.06)		L
HI 024124.0+262227	3.1, 68	10627(8, 0)	255(12)	1.73	0.98(0.13)		L
HI 024416.4+260648	2.4, 39	10571(7,11)	181(19)	2.36	1.29(0.15)		*
HI 024600.5+280145	1.5, 26	7959(4, 0)	354(6)	2.84	4.12(0.39)		*

Table 2—Continued

Source	$\epsilon_\alpha, \epsilon_\delta$ sec, "	$cz_\odot(\epsilon_{cz})$ km s^{-1}	$W(\epsilon_w)$ km s^{-1}	rms mJy	$F_c(\epsilon_f)$ Jy km s^{-1}	F_m Jy km s^{-1}	Notes
HI 024609.7+270247	1.0, 14	5732(6, 0)	225(8)	2.50	4.22(0.33)	5.30	*
HI 024752.7+270607	10.0, 15	5845(5, 0)	119(7)	6.47	2.78(0.30)		*
HI 025122.4+263459	1.3, 21	7489(5, 0)	136(7)	3.06	2.48(0.21)	3.57	*
HI 025149.8+260303	2.9, 59	10175(10, 0)	190(14)	3.12	2.34(0.25)		L
HI 030942.0+262649	2.3, 55	10783(6,51)	170(73)	2.54	0.94(0.14)		L
HI 031952.6+262935	2.0, 29	11053(7, 0)	121(10)	2.91	1.63(0.16)		L
HI 032120.9+262104	3.0, 47	11358(4,56)	251(79)	2.55	1.39(0.19)		L
HI 033140.7+260603	3.1, 43	10344(5, 0)	201(6)	2.12	0.88(0.12)		L
HI 033401.6+261019	4.9, 79	9997(5,55)	308(78)	2.22	1.90(0.22)		L
HI 033716.0+262357	5.9, 80	12015(14,66)	208(96)	2.11	0.81(0.15)		L *
HI 040226.1+264950	0.8, 16	5652(6,19)	93(28)	2.72	0.93(0.11)		L *
HI 040328.6+262149	2.6, 30	7072(7, 0)	379(10)	2.43	2.43(0.29)		*
HI 041559.8+265855	1.8, 20	3673(7, 0)	171(10)	2.85	2.20(0.21)		L
HI 041844.5+265513	1.9, 28	7582(12,16)	279(28)	2.62	3.14(0.31)		
HI 041904.2+261210	2.9, 44	3760(4, 0)	255(5)	2.07	4.95(0.37)		*
HI 042739.5+260545	4.4, 96	1936(9,26)	70(39)	3.28	1.13(0.11)		L *
HI 060125.5+260524	1.1, 75	5934(5, 0)	246(7)	3.71	4.77(0.42)		*
HI 060628.3+262314	0.7, 11	2724(3, 0)	196(4)	2.81	5.51(0.42)	6.20	*
HI 062218.4+262631	2.7, 48	6196(8, 0)	215(11)	2.49	1.69(0.19)		*
HI 063337.5+262911	1.3, 19	3404(4, 8)	203(12)	2.37	2.10(0.19)	3.13	
HI 063840.8+263006	2.4, 32	9821(8, 0)	308(11)	2.82	4.04(0.36)		*
HI 065004.2+262342	4.0, 56	9508(7, 0)	361(10)	2.67	2.34(0.30)		*

Table 3. Parameters of LBW Detections

Source	R. A. hhmmss.s	Dec. ddmmss	$cz_\odot(\epsilon_{cz})$ km s^{-1}	$W(\epsilon_w)$ km s^{-1}	rms mJy	$F_c(\epsilon_f)$ Jy km s^{-1}	Notes
HI 001709.7+271616	001713.3	+271454	3710(9, 0)	150(13)	2.08	1.46(0.15)	*
HI 002115.8+262318	002115.3	+262307	9191(5,16)	126(23)	2.27	0.78(0.10)	*
HI 002905.0+272936	002905.0	+272914	8710(5, 0)	104(7)	1.42	1.27(0.10)	*
HI 003027.1+263852	003026.8	+263833	9668(5, 0)	255(7)	1.84	2.63(0.22)	
HI 003052.6+272328	003051.4	+272324	11287(8, 0)	127(12)	1.28	0.97(0.10)	
HI 003831.2+262132	003832.3	+262050	7220(7, 0)	88(9)	2.10	0.79(0.09)	
HI 004113.4+272248	004113.0	+272220	10348(15, 0)	292(21)	1.95	2.59(0.26)	
HI 004629.4+264134	004627.7	+264131	5086(4,16)	82(23)	1.27	0.36(0.04)	
HI 004645.5+275553	004647.1	+275634	6896(10,53)	289(76)	1.14	1.20(0.30)	*
HI 005124.7+271517	005123.4	+271617	4523(6, 0)	93(8)	1.41	0.72(0.07)	
HI 005305.3+272909	005307.8	+272909	4751(3, 0)	61(4)	1.75	1.48(0.12)	*
HI 010032.5+270540	010034.0	+270553	11050(8, 0)	186(11)	1.50	2.06(0.18)	
HI 010225.7+263613	010224.0	+263719	5007(11, 0)	229(16)	1.31	1.14(0.13)	*
HI 010318.1+264747	010317.8	+264747	5081(10,14)	135(24)	1.12	0.74(0.07)	*
HI 010456.8+264942	010456.5	+264942	14271(12, 0)	269(16)	1.21	1.41(0.14)	
HI 010654.5+263054	010700.8	+263054	10149(9, 0)	121(13)	2.14	1.27(0.13)	
HI 010703.4+271516	010703.2	+271516	10127(6, 0)	132(9)	1.87	0.61(0.08)	
HI 011302.6+273832	011257.5	+273758	4961(4, 0)	33(6)	1.00	0.37(0.03)	*
HI 011643.2+265307	011643.0	+265445	12312(7,20)	144(29)	1.36	0.71(0.07)	
HI 013152.5+271912	013154.0	+271944	3823(5, 0)	38(7)	1.44	0.57(0.05)	
HI 013339.0+262439	013339.2	+262513	11108(9, 0)	256(12)	1.02	1.01(0.10)	
HI 013740.2+271042	013743.7	+271050	11091(6, 0)	363(8)	1.60	2.29(0.22)	
HI 014105.8+272007	014108.0	+271920	282(2, 0)	27(3)	1.61	0.59(0.05)	*
HI 014331.2+275930	014327.0	+280002	10136(9, 0)	276(12)	1.24	1.68(0.15)	
HI 014455.3+272942	014454.1	+272909	12837(6, 0)	494(9)	0.86	0.85(0.12)	*
HI 015047.7+271714	015046.6	+271641	14632(9, 0)	340(12)	0.86	0.77(0.10)	
HI 015150.7+274448	015152.7	+274531	10715(10, 0)	95(15)	1.85	1.12(0.11)	
HI 015439.1+274824	015438.9	+274919	14870(9, 9)	189(18)	1.70	1.31(0.13)	
HI 015439.8+271111	015440.0	+271110	8435(15, 0)	311(21)	1.61	1.72(0.19)	*
HI 015857.7+265710	015859.4	+265749	13046(6, 0)	45(9)	1.94	0.92(0.08)	
HI 015917.6+270027	015919.2	+270044	5324(8,16)	109(25)	1.96	1.03(0.10)	*
HI 020304.8+271222	020303.0	+271316	4689(8, 0)	271(12)	1.21	0.63(0.10)	
HI 020329.8+273909	020328.8	+273860	16920(10, 0)	80(14)	1.77	0.94(0.09)	
HI 020530.0+272806	020533.3	+272755	12026(10,45)	299(65)	0.94	0.95(0.10)	
HI 020913.9+264536	020918.5	+264528	12761(8,112)	295(159)	1.65	1.00(0.15)	*
HI 020954.1+273147	020956.3	+273234	4919(9, 0)	98(13)	1.44	1.00(0.09)	
HI 021309.0+274650	021307.3	+274653	13093(9, 0)	203(13)	1.60	0.86(0.11)	
HI 021404.3+275302	021405.8	+275034	575(5, 0)	107(6)	1.58	1.59(0.13)	*
HI 021510.4+262415	021508.1	+262313	4996(7, 0)	188(11)	1.63	1.13(0.12)	
HI 021640.8+260835	021639.7	+260816	11339(8,56)	240(79)	1.33	0.88(0.10)	
HI 022103.9+270204	022101.0	+270204	10783(15,66)	330(96)	1.56	1.02(0.15)	*
HI 022138.2+280302	022139.7	+280307	10649(8, 0)	298(12)	1.69	2.26(0.21)	
HI 022345.8+262214	022347.5	+262207	9556(21, 0)	196(30)	0.81	0.62(0.07)	
HI 022405.6+263900	022406.5	+263960	9230(5, 0)	62(7)	1.65	0.45(0.05)	*
HI 022542.3+265853	022545.2	+265824	10001(5, 0)	239(7)	1.74	1.06(0.13)	
HI 022558.5+271607	022558.7	+271613	10217(7, 0)	356(9)	1.47	1.02(0.15)	*
HI 022740.9+265524	022738.5	+265445	10545(3, 0)	170(4)	1.76	1.42(0.13)	
HI 022751.5+275429	022754.1	+275419	10529(11, 0)	394(16)	1.40	1.83(0.20)	*

Table 3—Continued

Source	R. A. hhmmss.s	Dec. ddmmss	$cz_{\odot}(\epsilon_{cz})$ km s^{-1}	$W(\epsilon_w)$ km s^{-1}	rms mJy	$F_c(\epsilon_f)$ Jy km s^{-1}	Notes
HI 022900.2+263041	022859.4	+263242	9479(14, 0)	153(19)	1.92	0.93(0.12)	
HI 022901.5+260509	022901.5	+260448	5907(6, 0)	98(8)	1.78	1.18(0.10)	
HI 022919.3+272107	022919.9	+272116	1551(3, 0)	32(4)	1.11	0.49(0.04)	
HI 023138.9+271130	023139.5	+271046	980(5, 0)	27(7)	2.54	0.56(0.07)	
HI 023203.1+261156	023207.6	+261140	10810(11, 0)	106(16)	1.63	1.01(0.09)	
HI 023234.8+275608	023233.7	+275628	4657(9, 0)	145(13)	1.38	0.99(0.09)	
HI 023325.2+271204	023328.5	+271139	5341(7, 0)	203(10)	1.03	1.39(0.11)	
HI 023329.2+270136	023332.3	+270113	1668(6, 0)	71(8)	1.28	0.91(0.07)	
HI 024055.2+264046	024055.6	+264005	1499(6, 0)	44(9)	1.69	0.71(0.07)	
HI 024124.0+262227	024124.5	+262321	10633(5, 0)	255(7)	0.96	1.05(0.10)	
HI 025149.8+260303	025150.0	+260310	10173(5, 0)	186(7)	1.62	2.31(0.19)	
HI 030942.0+262649	030942.3	+262613	10830(6, 0)	121(9)	1.57	0.88(0.09)	
HI 031952.6+262935	031955.0	+262945	11068(4, 0)	143(6)	1.66	1.71(0.14)	
HI 032120.9+262104	032121.6	+262034	11351(14, 0)	314(20)	1.57	1.29(0.16)	
HI 033140.7+260603	033141.6	+260515	10338(14, 0)	196(20)	1.53	1.34(0.14)	
HI 033401.6+261019	033401.5	+261033	10019(7, 0)	314(10)	0.94	1.52(0.13)	
HI 033716.0+262357	033722.5	+262505	12010(5, 0)	203(7)	0.91	0.40(0.06)	*
HI 040226.1+264950	040226.3	+264928	5648(4, 0)	83(6)	1.59	0.83(0.07)	*
HI 041559.8+265855	041600.0	+265934	3669(3, 0)	161(5)	1.56	2.08(0.16)	
HI 042739.5+260545	042741.8	+260345	1957(4, 0)	76(6)	1.23	0.96(0.08)	*

Table 4. Optical ID, Distances and HI Masses

Source	AGC	R. A. hhmmss.s	Dec. ddmmss	D_{cmb} Mpc	D_{pec} Mpc	$\log(M_{HI})$ $M_\odot$	Notes
HI 001709.7+271616	101815	001713.3	+271454	48.2	53.5	8.98	*
HI 002115.8+262318	101816	002115.3	+262307	126.8	129.5	9.62	*
HI 002312.5+272644	221	002310.9	+272555	51.6	56.8	9.35	*
HI 002818.8+272136	278	002819.2	+272208	132.6	135.1	10.18	*
HI 002905.0+272936	101817	002905.1	+272913	119.7	122.6	9.55	*
HI 003027.1+263852	101819	003026.8	+263833	133.5	136.0	10.04	
HI 003052.6+272328	101820	003051.4	+272324	156.3	158.5	9.76	
HI 003831.2+262132	101821	003832.3	+262050	98.5	102.1	9.25	
HI 003855.1+265753	100381	003855.7	+265758	69.3	74.0	9.40	*
HI 004034.8+270239	101822	004036.4	+270302	68.7	73.4	9.63	*
HI 004113.4+272248	101823	004113.0	+272220	143.2	145.5	10.02	
HI 004256.8+271522	100482	004257.9	+271512	71.0	75.5	9.68	*
HI 004357.1+260731	100489	004357.9	+260849	65.5	70.2	8.95	*
HI 004404.2+261243	469	004403.7	+261227	139.5	141.9	9.97	*
HI 004411.5+265042	470	004412.5	+265045	69.7	74.2	10.18	
HI 004456.0+272758	100499	004456.7	+272656	69.8	74.3	9.15	*
HI 004629.4+264134	101825	004627.7	+264131	68.1	72.8	8.98	
HI 004645.5+275553	100550	004647.0	+275630	95.0	98.6	9.72	*
HI 004650.7+262846	483	004650.3	+262831	66.3	71.0	9.49	*
HI 004716.1+274854	489	004718.6	+274938	63.3	68.0	9.41	*
HI 004738.1+264856	101826	004737.7	+264819	66.2	70.9	9.25	
HI 004803.3+273717	491	004801.5	+273728	66.2	70.8	9.59	*
HI 004816.9+262806	100573	004816.6	+262802	70.7	75.3	9.09	*
HI 004834.5+274100	497	004834.9	+274130	70.0	74.4	9.67	*
HI 005009.5+271328	101827	005012.2	+271325	65.8	70.4	9.09	*
HI 005124.7+271517	101828	005124.7	+271601	60.2	64.9	8.74	
HI 005305.3+272909	101829	005307.8	+272909	63.4	68.1	9.17	*
HI 010032.5+270540	101685	010034.0	+270553	152.8	155.0	10.05	
HI 010158.0+263010	100714	010158.4	+262912	139.3	141.7	9.56	*
HI 010225.7+263713	100719	010224.0	+263717	66.6	71.1	9.19	*
HI 010318.1+264747	112506	010317.8	+264747	68.1	72.5	9.22	*
HI 010456.8+264942	112507	010456.5	+264942	199.5	201.4	10.08	
HI 010654.5+263054	112508	010700.8	+263054	140.6	142.9	9.68	
HI 010703.4+271516	112509	010703.2	+271516	140.2	142.5	9.66	
HI 011302.6+273832	112510	011257.4	+273759	66.6	70.8	8.56	*
HI 011443.5+270813	110150	011445.6	+270809	47.5	52.2	9.49	*
HI 011643.2+265307	112511	011643.0	+265445	171.2	173.1	9.62	
HI 011743.9+270006	112512	011742.4	+270033	169.3	171.2	10.02	*
HI 012242.5+265157	110263	012241.8	+265203	125.3	127.8	9.75	*
HI 012403.9+270300	948	012404.1	+270246	66.1	70.2	9.34	*
HI 012405.2+280433	112513	012403.6	+280557	54.2	58.5	9.27	*
HI 012607.5+275810	110324	012608.8	+275756	53.4	57.7	8.84	*
HI 012944.1+272249	112515			176.5	178.4	10.28	*
HI 013152.5+271912	112516	013154.0	+271945	50.6	54.9	8.59	
HI 013315.1+261438	112518	013315.6	+261455	95.3	98.5	9.75	
HI 013339.0+262439	112519	013339.2	+262513	154.4	156.5	9.73	
HI 013716.0+262606	110443	013715.3	+262611	51.4	55.6	8.81	*
HI 013740.2+271042	112520	013743.7	+271040	154.3	156.3	10.00	

Table 4—Continued

Source	AGC	R. A. hhmmss.s	Dec. ddmmss	D_{cmb} Mpc	D_{pec} Mpc	$\log(M_{HI})$ $M_\odot$	Notes
HI 014105.8+272007	112521	014108.0	+271920		6.3	6.77	*
HI 014147.3+273159	110477	014146.4	+273012	150.7	152.7	9.76	*
HI 014214.9+262202	110482	014217.3	+262200	1.2	7.4	7.13	*
HI 014331.2+275930	111466	014327.0	+280004	141.5	143.5	9.94	
HI 014428.3+275522	110790	014428.8	+275544	53.9	57.8	9.79	*
HI 014441.4+271707	111945	014442.7	+271718	2.2	8.2	7.66	*
HI 014455.3+272942	112522	014454.1	+272909	178.9	180.8	9.79	*
HI 014640.9+264754	111946	014642.2	+264805	1.3	7.5	6.95	*
HI 014653.7+280448	111332	014654.2	+280558	47.5	51.4	9.23	*
HI 014724.3+275312	1250	014725.0	+275309	49.0	53.0	9.42	*
HI 014729.9+271958	1249	014729.9	+271958	1.1	7.2	8.82	*
HI 014753.9+272555	1256	014753.9	+272555	2.3	8.3	9.05	*
HI 014837.9+273259	110535	014835.2	+273253	153.5	155.4	10.22	*
HI 014915.3+274248	110543	014920.1	+274244	149.8	151.8	10.01	*
HI 015011.6+271145	1291	015012.3	+271145	46.3	50.2	9.61	*
HI 015013.0+273842	1292	015014.0	+273845	46.7	50.7	9.94	*
HI 015047.7+271714	112523	015046.6	+271641	205.1	206.9	9.82	
HI 015150.7+274448	112524	015152.7	+274531	149.7	151.7	9.72	
HI 015439.1+274824	112525	015438.9	+274919	208.2	210.0	10.13	
HI 015439.8+271111	112526	015440.0	+271110	116.6	118.9	9.62	*
HI 015519.2+275645	111977	015520.4	+275713		5.5	6.75	*
HI 015536.6+274154	112527	015535.6	+274328	115.6	117.9	9.70	
HI 015751.8+264537	112528	015752.2	+264543	173.9	175.7	10.27	
HI 015857.7+265710	112529	015859.6	+265749	182.6	184.4	9.75	
HI 015917.6+270027	112459	015919.2	+270044	72.1	75.3	9.11	*
HI 015937.0+272555	110716	015938.1	+272601	71.6	74.7	9.58	*
HI 015952.5+262407	112530	015953.0	+262416	70.9	74.1	9.53	*
HI 020133.9+262914	1507	020130.8	+262851	69.9	73.1	9.92	*
HI 020144.4+263227	1510	020146.3	+263246	67.9	71.1	9.80	*
HI 020248.2+263434	1533	020248.1	+263452	204.9	206.7	10.70	*
HI 020304.8+271222	122180			64.7	67.9	8.85	*
HI 020329.8+273909	122181	020328.8	+273900	238.4	240.1	10.00	*
HI 020343.0+261608	120005	020341.0	+261636	67.8	71.0	9.01	*
HI 020353.5+261719	122182	020358.3	+261611	68.6	71.7	8.90	*
HI 020430.7+275454	1565	020432.0	+275531	63.6	66.7	9.68	*
HI 020530.0+272806	122183	020533.3	+272755	167.3	169.1	9.90	
HI 020558.3+272121	122185	020600.8	+272128	66.9	69.9	9.34	
HI 020626.5+270152	1595	020627.3	+270159	67.4	70.4	9.68	*
HI 020902.1+273202	120055	020902.4	+273210	137.3	139.3	9.87	*
HI 020913.9+264536	122186	020918.5	+264528	179.1	180.8	10.02	*
HI 020954.1+273147	122187	020956.3	+273234	66.6	69.5	9.02	*
HI 021309.0+274650	122188	021307.3	+274653	183.8	185.5	10.21	
HI 021328.9+263102	122189	021331.2	+263049	202.6	204.4	10.44	
HI 021404.3+275302	1718	021403.6	+275236	4.9	10.4	8.20	*
HI 021510.4+262415	122190	021508.1	+262313	67.8	70.7	9.15	
HI 021640.8+260835	122191	021639.7	+260816	158.6	160.4	9.79	
HI 022102.1+274615	122192	022103.4	+274526	132.8	134.7	10.05	*
HI 022103.9+270204	122193	022101.1	+270204	150.8	152.6	9.76	*

Table 4—Continued

Source	AGC	R. A. hhmmss.s	Dec. ddmmss	D_{cmb} Mpc	D_{pec} Mpc	$\log(M_{HI})$ $M_\odot$	Notes
HI 022138.2+280302	122194	022139.8	+280307	149.1	150.8	10.02	
HI 022224.8+262552	122195	022226.1	+262610	155.7	157.5	10.21	*
HI 022335.8+271851	120201	022331.3	+271924	148.9	150.7	9.59	*
HI 022340.2+270927	1844	022339.4	+270932	148.9	150.6	9.99	*
HI 022345.8+262214	122196	022347.5	+262207	133.2	135.1	9.59	
HI 022348.9+272848	1848	022355.5	+272932	149.7	151.5	10.13	*
HI 022355.8+270618	1850	022358.5	+270700	74.8	77.1	9.15	*
HI 022405.6+263900	122197			128.4	130.3	9.44	*
HI 022459.4+260314	120218	022500.2	+260301	140.9	142.7	9.93	*
HI 022533.4+264458	1881	022535.2	+264436	144.6	146.4	9.98	*
HI 022538.8+271709	120234	022539.5	+271743	125.1	127.0	10.01	*
HI 022542.3+265853	122198	022545.2	+265824	139.1	140.9	9.80	
HI 022558.5+271607	121216	022558.7	+271613	142.6	144.3	10.11	*
HI 022609.4+273549	1892	022612.5	+273610	139.4	141.2	9.90	*
HI 022617.1+260750	120244	022615.2	+260623	143.0	144.8	9.79	*
HI 022620.2+271315	1894	022616.8	+271242	145.0	146.7	9.67	*
HI 022629.9+273937	1899	022626.2	+273913	135.4	137.2	9.66	*
HI 022632.1+274941	1902	022633.7	+274926	134.2	136.0	10.00	*
HI 022740.9+265524	122199	022738.5	+265445	147.3	149.1	9.65	
HI 022741.1+271328	120265	022740.9	+271315	69.9	72.2	8.99	*
HI 022742.7+261406	120266	022742.3	+261334	132.4	134.2	10.03	*
HI 022745.2+263507	1921	022746.4	+263520	136.7	138.5	9.72	*
HI 022751.5+275429	121307	022754.9	+275422	147.5	149.3	9.83	*
HI 022816.3+261854	1939	022817.6	+261844	71.6	74.0	10.20	*
HI 022850.0+264500	122200	022849.0	+264450	132.8	134.6	9.94	
HI 022900.2+263041	122201	022859.4	+263242	132.2	134.0	9.48	
HI 022901.5+260509	122202	022901.5	+260448	81.1	83.3	9.21	
HI 022919.3+272107	122203	022919.9	+272116	18.9	22.9	7.85	
HI 023023.1+275653	122204	023024.1	+275736	64.5	66.7	9.07	
HI 023052.0+261047	120299	023050.4	+261136	186.7	188.4	10.32	*
HI 023058.9+275709	122206	023100.3	+275730	19.5	23.4	8.58	
HI 023103.8+274053	1990	023104.1	+274158	61.7	64.0	9.00	*
HI 023121.5+261239	122207	023122.1	+261152	32.7	36.0	9.00	
HI 023124.6+264706	122208	023124.5	+264717	153.5	155.3	10.42	
HI 023133.0+264727	122210	023133.0	+264752	61.8	64.2	9.20	
HI 023135.9+263155	122211	023136.8	+263230	49.6	52.2	8.72	
HI 023137.5+261010	120307	023134.6	+260958	152.0	153.8	10.29	*
HI 023138.9+271130	122212	023139.3	+271045	10.8	15.4	7.46	
HI 023203.1+261156	122213	023207.6	+261140	151.1	152.8	9.64	
HI 023234.8+275608	122214	023233.7	+275628	63.4	65.6	9.04	
HI 023325.2+271204	122215	023328.5	+271139	73.2	75.3	9.26	
HI 023329.2+270136	122217	023332.3	+270113	20.5	24.4	8.04	
HI 023516.3+280108	122218	023515.2	+280116	35.4	38.3	9.10	
HI 023851.0+275109	2134	023851.9	+275048	62.5	64.5	10.05	*
HI 024055.2+264046	122219	024055.6	+264005	18.1	22.0	7.80	
HI 024124.0+262227	122220	024124.5	+262321	148.7	150.3	9.72	
HI 024416.4+260648	122221	024418.5	+260629	147.9	149.5	9.83	*
HI 024600.5+280145	120490	024601.1	+280140	110.6	112.2	10.09	*

Table 4—Continued

Source	AGC	R. A. hhmmss.s	Dec. ddmmss	D_{cmb} Mpc	D_{pec} Mpc	$\log(M_{HI})$ $M_\odot$	Notes
HI 024609.7+270247	2236	024611.1	+270239	78.8	80.4	9.91	*
HI 024752.7+270607	2272	024804.5	+270609	80.5	82.0	9.64	*
HI 025122.4+263459	122223	025123.1	+263458	104.0	105.4	9.97	*
HI 025149.8+260303	122224	025150.0	+260310	142.4	143.9	10.06	
HI 030942.0+262649	131043	030942.3	+262613	151.4	152.8	9.71	
HI 031952.6+262935	131044	031955.5	+262936	155.4	156.8	9.97	
HI 032120.9+262104	131045	032121.6	+262034	159.8	161.1	9.93	
HI 033140.7+260603	131046	033141.6	+260515	145.5	146.6	9.65	
HI 033401.6+261019	131047	033401.5	+261033	140.6	141.7	9.95	
HI 033716.0+262357	131048	033722.5	+262505	169.5	170.7	9.75	*
HI 040226.1+264950	130368	040226.3	+264928	79.1	77.9	9.12	*
HI 040328.6+262149	140002	040329.8	+262146	99.4	98.8	9.75	*
HI 041559.8+265855	140472	041559.7	+265955	51.0	49.6	9.11	
HI 041844.5+265513	140473	041843.8	+265526	106.9	106.3	9.92	
HI 041904.2+261210	3009	041905.9	+261048	52.3	50.8	9.48	*
HI 042739.5+260545	140474	042743.5	+260437	26.5	26.8	8.28	*
HI 060125.5+260524	150264	060126.6	+260328	85.5	81.3	9.87	*
HI 060628.3+262314	160446	060628.9	+262346	39.7	36.5	9.29	*
HI 062218.4+262631	160544			89.6	85.5	9.46	*
HI 063337.5+262911	160545	063339.0	+262905	50.0	45.6	9.19	
HI 063840.8+263006	160122	063838.1	+263022	141.7	140.8	10.28	*
HI 065004.2+262342	160242	065004.2	+262248	137.5	136.3	10.01	*